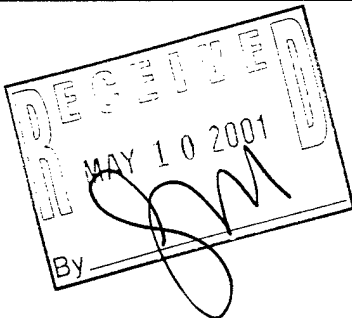


# REPORT DOCUMENTATION PAGE

Form Approved  
OMB NO. 0704-0188

Public Reporting burden for this collection of information is estimated to average 1 hour per response, including the time for reviewing instructions, searching existing data sources, gathering and maintaining the data needed, and completing and reviewing the collection of information. Send comment regarding this burden estimates or any other aspect of this collection of information, including suggestions for reducing this burden, to Washington Headquarters Services, Directorate for information Operations and Reports, 1215 Jefferson Davis Highway, Suite 1204, Arlington, VA 22202-4302, and to the Office of Management and Budget, Paperwork Reduction Project (0704-0188,) Washington, DC 20503.

1. AGENCY USE ONLY (Leave Blank)		2. REPORT DATE April 27, 2001		Final Report 7/1/98 - 6/30/00	
4. TITLE AND SUBTITLE Low Power, Low Cost, Long Wavelength VCSELs for Optical Interconnects				DAAG55-98-1-0437	
6. AUTHOR(S) J. S. Harris					
Stanford University				8. PERFORMING ORGANIZATION REPORT NUMBER	
9. SPONSORING / MONITORING AGENCY NAME(S) AND ADDRESS(ES) U. S. Army Research Office P.O. Box 12211 Research Triangle Park, NC 27709-2211				10. SPONSORING / MONITORING AGENCY REPORT NUMBER  38865.2-EL	
11. SUPPLEMENTARY NOTES The views, opinions and/or findings contained in this report are those of the author(s) and should not be construed as an official Department of the Army position, policy or decision, unless so designated by other documentation.					
12 a. DISTRIBUTION / AVAILABILITY STATEMENT Approved for public release; distribution unlimited.				12 b. DISTRIBUTION CODE	
13. ABSTRACT (Maximum 200 words)  See attached  					
14. SUBJECT TERMS				15. NUMBER OF PAGES 424	
				16. PRICE CODE	
17. SECURITY CLASSIFICATION OR REPORT UNCLASSIFIED	18. SECURITY CLASSIFICATION ON THIS PAGE UNCLASSIFIED	19. SECURITY CLASSIFICATION OF ABSTRACT UNCLASSIFIED	20. LIMITATION OF ABSTRACT UL		

NSN 7540-01-280-5500

Standard Form 298 (Rev.2-89)  
Prescribed by ANSI Std. Z39-18  
298-102

20010516 154

**Low Power, Low Cost, Long Wavelength  
VCSELs for Optical Interconnects**

**Final Report  
April 2001**

**U. S. Army Research Office  
DAAG55-98-1-0437**

**J. S. Harris, Principal Investigator  
Stanford University**

**Approved for Public Release  
Distribution Unlimited**

The views, opinions, and/or findings contained in this report are those of the authors and should not be construed as an official Department of the Army position, policy or decision unless so designated by other documentation.

# **Low Power, Low Cost, Long Wavelength VCSELs for Optical Interconnects**

## **1. Overview**

Vertical Cavity Surface-Emitting Lasers (VCSELs) will be important in large-scale optical interconnection schemes because of the ability to fabricate large arrays of devices at a low cost. Long wavelength VCSELs offer many performance advantages for optical interconnects compared to their shorter wavelength near-IR counterparts, including lower voltage and power. Until recently, it has not been feasible to fabricate long-wavelength ( $>1300\text{nm}$ ) VCSELs due to fundamental materials limitations in the InP based system. The first breakthrough in potentially realizing long wavelength VCSELs on GaAs substrates was the work on GaInNAs by Kondow, et al (1). Subsequently, M. Larson, working with Kondow demonstrated the first long wavelength optically pumped GaInNAs VCSEL (2) and electrically pumped VCSEL (3). The exciting potential of these lasers is fivefold: 1) extension of VCSEL technology across the entire  $1.3\text{-}1.6\mu\text{m}$  communications band, 2) high temperature operation and high  $T_0$ , 3) low power, 4) low cost 5) monolithic integration with GaAs electronics. Seeing the tremendous potential for this new alloy material, we initiated a new effort at Stanford University to improve the performance of GaInNAs lasers to levels comparable to or better than shorter wavelength near-IR VCSELs. This report details the work of that effort which resulted in the first cw, room temperature GaInNAs VCSEL operating at  $>1.2\mu\text{m}$ .

## **2. Introduction**

Due to their excellent performance and low cost, vertical cavity surface emitting lasers will enable high volume applications, such as large scale free space optical interconnection for chip to chip and board to board applications as well as very high bandwidth local and metro area network applications. The threshold currents are becoming low enough in VCSELs to allow direct digital modulation by low power CMOS circuitry without any DC bias. These devices can be fabricated with high yield and low cost due the use of well developed GaAs technology that is nearly identical to that employed in making light emitting diodes. Large arrays are possible providing many data paths in a small area. Unfortunately, current low cost GaAs based VCSELs are still less than optimal from a systems perspective since the drive voltages are fairly high relative to that of the ever decreasing CMOS voltages. In the high density optical interconnection of Si CMOS circuitry using VCSEL arrays, having VCSEL drive voltages compatible with CMOS voltages is extremely important because it greatly simplifies the system/circuit design. Since CMOS voltages are continuing to decrease, it is important to push the drive voltage of VCSELs lower as well. Low

voltage also translates into lower power consumption which is also an important issue for high density interconnects and direct CMOS drive applications, as well as other low power applications, such as in aerospace and mobile systems.

The physics of diode lasers dictates that the applied voltage needs to be at least equal to the bandgap of the semiconductor to achieve population inversion and lasing threshold. Because of the reduced bandgap, long wavelength VCSELs offer the possibility of lower threshold voltages than their near-IR counterparts (less than one volt compared to 1.4-1.5 volts). Therefore, to achieve lower voltage and lower power VCSELs, the wavelength of emission needs to be pushed to long wavelengths such as 1.3 $\mu\text{m}$  or 1.55 $\mu\text{m}$ . The reason for these wavelengths is the added benefit of compatibility with low loss optical fiber systems.

Another benefit of the longer wavelength VCSELs is the optical transparency of GaAs and Si substrates, which makes more integration options possible. For example, in free space applications, micro-lens arrays are needed to overcome diffraction from the small diameter lasers. The alignment of micro-lens arrays with VCSEL arrays is a significant problem because of the small size of both the VCSELs and lenses and the close spacing of the devices in large VCSEL arrays. By fabricating the lens array lithographically on the backside of the transparent substrate on which the devices were grown or bonded, the lenses are inherently aligned to the devices, reducing the number of complex alignment steps in system fabrication.

As mentioned previously, developing 1.3 $\mu\text{m}$  and 1.5 $\mu\text{m}$  VCSELs has the added benefit of being compatible with optical fiber systems. The advantages of being compatible with fiber systems are several fold. First, more universal or standard products can be developed which should make them less expensive. Second, if optical interconnects are used inside of computers, no wavelength conversion will be needed when the computer talks to the outside world via fiber. For fiber based applications, the properties of silica fiber at 0.85 $\mu\text{m}$  and 0.98 $\mu\text{m}$  limit transmission to about 1 Gb/s over a distance of about 500 meters. Many fiber applications will certainly need longer distances and higher data rates but will not justify the cost of high performance telecom lasers currently employed in long-haul fiber systems. Most large buildings, airplanes, and ships will have cable runs further than 500 meters. Low cost VCSELs operating at 1.3 $\mu\text{m}$  would enable such interconnects to be readily realized.

Unfortunately, it has been very difficult to make long-wavelength VCSELs. Because the refractive index contrast is insufficient in conventional materials grown on InP, there has been difficulty in making distributed Bragg reflector (DBR) mirrors of sufficient reflectivity. Also, the

threshold current in conventional long wavelength laser materials depends much more strongly on temperature than their shorter wavelength counterparts, requiring external cooling for systems applications. Such cooling systems drastically increase the total transmitter cost and size and limit the prospects of integration. For VCSELs, the thermal performance of the active regions is of utmost importance because of the parasitic DBR resistance and its associated power dissipation typical of many VCSEL designs.

Because of the problems with conventional materials, alternative materials schemes need to be employed. Our approach is to use the novel material system GaInNAs grown on GaAs to achieve long wavelength emission. This approach has already yielded electrically injected VCSELs in work done by one member of our team while in Japan [3,4]. The advantages of GaInNAs include excellent thermal performance and a device structure nearly identical to that of 0.98 $\mu$ m VCSELs with one epitaxial growth and high performance GaAs/AlAs mirrors. For these reasons, the cost of fabrication should be comparable to that of current near-IR VCSELs.

At the initiation of the program, an existing Applied EPI (formerly Varian) GEN II MBE system was modified by adding additional pumping capacity and a SVT RF plasma N source. Following this introduction, publications that describe the successful results of this project are presented. As can be seen from these publications, our goals of creating long wavelength VCSELs using GaInNAs active materials was successful. We demonstrated the first cw, room temperature GaInNA VCSEL operating at 1.2 $\mu$ m. With further optimization of the design and material issues we expect to be able to push the device operation to longer wavelengths and continue to decrease the operating threshold currents and voltage. GaInNAs promises to be a major player in the rapidly expanding optical data networks and interconnects areas.

We would like to acknowledge the vision and the support of Drs. Elias Towe and Robert Leheny at DARPA and Dr. Mitra Dutta at ARO who helped make the advances described here possible.

### **Publications**

1. C. W. Coldren, S. G. Spruytte, M. C. Larson and J. S. Harris, "Group III-Nitride-Arsenide Long Wavelength Lasers Grown by Elemental Source Molecular Beam Epitaxy," *Proceedings of LEOS Annual Meeting*, San Francisco, Nov. 1999, 457-458.

2. M. C. Larson, C. W. Coldren, S. G. Spruytte, H. E. Petersen and J. S. Harris, "Low Threshold Current Continuous-Wave GaInNAs/GaAs VCSELs," *Proceedings of CLEO 2000*, San Francisco, April 2000, 9-10.
3. C. W. Coldren, S. G. Spruytte, M. C. Larson and J. S. Harris, "Group III-Nitride-Arsenide Long Wavelength Lasers Grown by Elemental Source Molecular Beam Epitaxy," *J. Vac. Sci. Technol. B*, **18**(3), May/Jun 2000, 1480-1483.
4. C. W. Coldren, M. C. Larson, S. G. Spruytte and J. S. Harris, "1200nm GaAs-based Vertical Cavity Lasers Employing GaInNAs Multi-quantum Well Active Regions," *Electronics Letters*, **36**(11), 5/25/00, 951-952.
5. P. Krispin, S. G. Spruytte, J. S. Harris and K. H. Ploog, "Electrical Depth Profile of p-type GaAs/Ga(As, N)/GaAs Heterostructures Determined by Capacitance-voltage Measurements," *J. of Appl. Phys.*, **88**(7), October 1, 2000, 4153-4158.
6. M. C. Larson, C. W. Coldren, S. G. Spruytte, H. E. Petersen and J. S. Harris, "Low-threshold Oxide-confined GaInNAs Long Wavelength Vertical Cavity Lasers," *IEEE Photonics Technology Letters*, **12**(12), December 2000, 1598-1600.
7. S. G. Spruytte, "MBE Growth of Nitride-arsenides for Long Wavelength Opto-Electronics," Ph.D. Thesis, April 2001.

#### **Scientific Personnel**

S. Spruytte, Ph.D., April 2001

C. W. Coldren

J. S. Harris

## Group III-Nitride-Arsenide Long Wavelength Lasers Grown by Elemental Source Molecular Beam Epitaxy

C.W. Coldren, S.G. Spruytte, J.S. Harris  
Solid State and Photonics Laboratory  
Stanford University

Via Ortega, Stanford, CA. 94305  
Tel: 650-725-8313 Fax: 650-723-4659 email: cwc@snow.stanford.edu

M.C. Larson  
Lawrence Livermore National Laboratory

**Abstract:** Employing group III-arsenide-nitride materials, low wavelength active regions with emission at 1.3 $\mu$ m have been developed on GaAs substrates. Broad area, single quantum well, in-plane lasers with thresholds as low as 1.1kA/cm<sup>2</sup> were fabricated.

Low cost lasers operating beyond 1.2 $\mu$ m will enable higher performance local area network communications systems due to better fiber properties at the longer wavelengths compared to the shorter 850nm standard. Additionally, long distance WDM systems can benefit from low cost lasers with operating wavelengths around 1.3 $\mu$ m. Group III-nitride-arsenide active regions allow the fabrication of low cost, 1.2-1.3 $\mu$ m diode laser devices due to the use of GaAs substrates and AlGaAs materials which have a well developed fabrication technology. Low cost, vertical cavity laser fabrication at long wavelengths is also possible using nitride-arsenide active regions with (Al)GaAs DBR mirrors. The growth of the nitride-arsenides is complicated by both the difficulty in generating reactive nitrogen and the mismatch in properties of the nitride and arsenide materials. With optimized growth conditions it is possible, though, to grow laser diodes with low thresholds and good efficiencies.

Growth of group III-nitride-arsenide materials was performed by elemental source molecular beam epitaxy employing a nitrogen r.f. plasma cell (solid source group III, cracked arsenic, and atomic nitrogen). Initial growth studies determined both the proper growth conditions to obtain quality layers and the bandgaps of the grown materials as a function of nitrogen content. Emission at 1.3 $\mu$ m can be achieved in group III-nitride-arsenide quantum well materials grown on GaAs; shown in figure 1 is room temperature photoluminescence spectra for 6.5nm In<sub>0.3</sub>Ga<sub>0.7</sub>N<sub>0.02</sub>As<sub>0.98</sub> double quantum well structures. The as-grown emission spectrum has a peak at 1.3 $\mu$ m and improves dramatically with a small amount of thermal annealing (120s at 600C) and further improves with more substantial annealing (RTA).

TEM studies of the In<sub>0.3</sub>Ga<sub>0.7</sub>N<sub>0.02</sub>As<sub>0.98</sub> quantum wells (see figure 3) show the high crystal quality of the films.

Broad area single quantum well lasers were fabricated using single 7nm In<sub>0.3</sub>Ga<sub>0.7</sub>N<sub>0.02</sub>As<sub>0.98</sub> quantum wells embedded in the center of 200nm GaAs waveguide core regions. The upper and lower waveguide cladding layers were 1.5 $\mu$ m of Al<sub>0.33</sub>Ga<sub>0.67</sub>As with average dopings of  $5 \times 10^{17}$ cm<sup>-3</sup> Be and  $1 \times 10^{18}$ cm<sup>-3</sup> Si. With constant nitrogen content, the threshold of such lasers depends greatly on the operation of the nitrogen r.f. plasma. Initial growths resulted in threshold current densities of 5-6kA/cm<sup>2</sup> for 20 $\mu$ m wide and 800 $\mu$ m long devices. However, with modified nitrogen plasma operation conditions and improved growth procedures much better results were obtained, threshold current densities for 20 $\mu$ m wide and 800 $\mu$ m long devices were as low as 1.1kA/cm<sup>2</sup>. The pulsed L-I and emission spectrum are shown in figures 2&4. The emission wavelength of the active regions in the laser diode (about 1.25  $\mu$ m) is shorter than that of the quantum wells grown without the waveguide structure because of out-diffusion of both indium and nitrogen at the elevated growth temperatures used for the AlGaAs cladding layers. With slightly modified active regions and cladding layer growth protocol, 1.3 $\mu$ m laser emission is expected with improved threshold current densities.

InGaAs quantum well structures were investigated for the purpose of making long wavelength diode laser devices grown on GaAs substrates. The InGaAs quantum wells exhibited good optical properties at 1.3 $\mu$ m and single quantum well lasers were fabricated with low threshold current densities and good slope efficiencies.

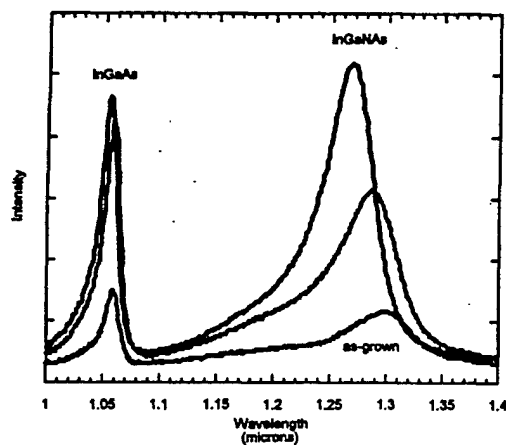


Figure 1: Room temperature photoluminescence of 6.5nm  $\text{In}_{0.3}\text{Ga}_{0.7}\text{N}_{0.02}\text{As}_{0.98}$  double quantum well structure. There are also two 6.5nm  $\text{In}_{0.3}\text{Ga}_{0.7}\text{As}$  quantum wells in the structure.

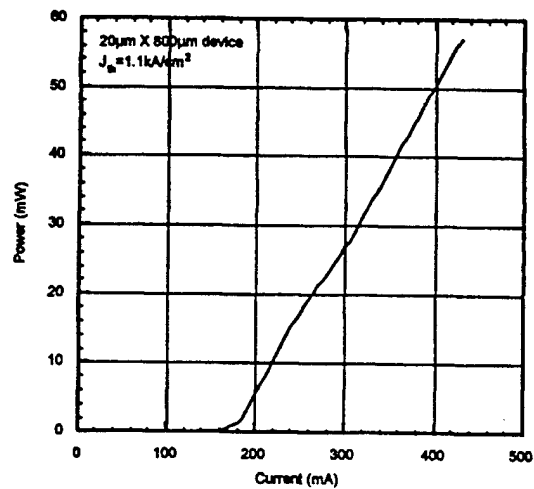


Figure 2:  $\text{In}_{0.3}\text{Ga}_{0.7}\text{N}_{0.02}\text{As}_{0.98}$  SQW laser L-I measured under pulsed operation (1ns pulses with 0.5% duty cycle).

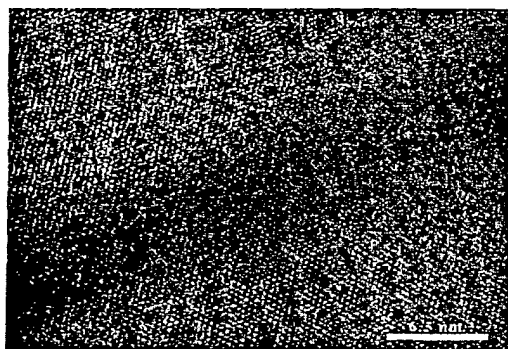


Figure 3: TEM of  $\text{In}_{0.3}\text{Ga}_{0.7}\text{N}_{0.02}\text{As}_{0.98}$  quantum well

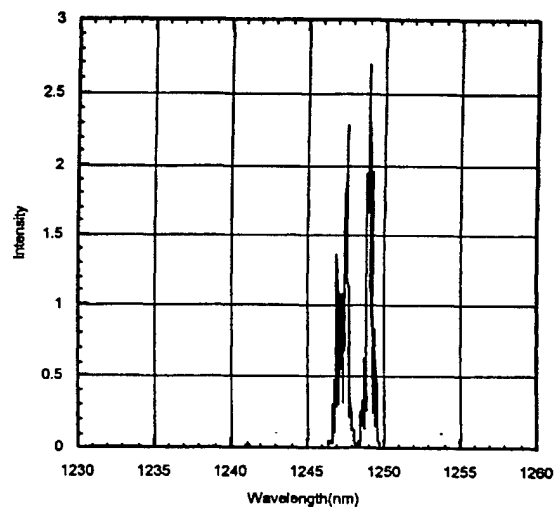


Figure 4:  $\text{In}_{0.3}\text{Ga}_{0.7}\text{N}_{0.02}\text{As}_{0.98}$  SQW laser optical spectrum

### Low Threshold Current Continuous-Wave GaInNAs /GaAs VCSELs

M.C. Larson<sup>1,3</sup>, C.W. Coldren<sup>1,2</sup>, S.G. Spruytte<sup>2</sup>, H.E. Petersen<sup>1</sup>, and J.S. Harris<sup>2</sup>

<sup>1</sup>Lawrence Livermore National Laboratory, P.O. Box 808, L-222, Livermore, CA 94551

<sup>2</sup>Solid State and Photonics Lab, Stanford University, CISX 126, Via Ortega, Stanford, CA 94305

Tel: 650-725-6909, Fax: 650-723-4659

<sup>3</sup>Presently with Agility Communications, 600 Pine Ave., Goleta, CA 93117 Tel: 805-690-1762

Tel: 805-690-1762

Vertical cavity surface-emitting lasers (VCSELs) emitting near 0.85  $\mu\text{m}$  are becoming increasingly important for short-haul optical fiber transmission systems. These devices benefit from highly reflective and thermally conductive all-epitaxial GaAs-based mirrors and efficient transverse confinement through AlAs-oxide dielectric apertures. Extending this commercially-established technology to wavelengths in the 1.3-1.6  $\mu\text{m}$  range allows for dramatically increased transmission bandwidth and distance in conventional single- and multi-mode fiber. GaInNAs is a promising active layer material grown on GaAs that can achieve 1.3  $\mu\text{m}$  emission [1], and electrically pulsed broad-area GaInNAs VCSELs [2,3] have been realized. Here we demonstrate for the first time low-threshold ( $\sim 1$  mA) GaInNAs VCSELs emitting at a wavelength of 1.2  $\mu\text{m}$  under continuous-wave room temperature operation.

The device structure is shown schematically in figure 1. The bottom mirror consists of a 22.5-period n-doped GaAs/AlAs distributed Bragg reflector (DBR) designed for a center wavelength  $\lambda$  near 1.2  $\mu\text{m}$ , the top mirror is a 20-period p-doped DBR whose reflectance is enhanced by a Ti/Au contact electrode, and the GaAs  $\lambda$  cavity contains three 70Å  $\text{Ga}_{0.3}\text{In}_{0.7}\text{N}_{0.02}\text{As}_{0.98}$  quantum wells (QWs) separated by 200Å GaAs barriers. The epilayers were grown by molecular beam epitaxy using solid-source arsenic and a rf nitrogen plasma source. After growth, the first 17 mirror periods of the top mirror were dry etched and subsequently capped with  $\text{SiO}_2$ , and the remaining three periods were etched to expose the AlAs for lateral oxidation, which formed square unoxidized apertures as small as 3.6  $\mu\text{m}$  on a side. After the top contact metalization, devices were mounted without heat sinking on a glass slide for optical emission through the substrate, which was contacted electrically with indium solder.

The output power and voltage vs. injection current (L-I-V) for devices of various aperture sizes were first characterized under pulsed operation (200 nsec at 10 kHz) as shown in figure 2. Pulsed threshold current varied from 0.89 mA for 3.6  $\mu\text{m}$  devices to approximately 21 mA for 29  $\mu\text{m}$  sizes. Threshold current density was within the range of 2-2.5  $\text{kA}/\text{cm}^2$  at larger sizes, and slope efficiency above 0.09 W/A was achieved. Threshold voltage above 10 V likely resulted from unoptimized doping and composition profiles at the heterointerfaces of the p-DBR. Next, similar measurements were taken for devices biased under CW operation, and are shown in figure 3. CW laser oscillation was achieved for aperture sizes ranging from 3.6  $\mu\text{m}$  to 6.4  $\mu\text{m}$ , with threshold currents from 0.94 to 2.3 mA and slope efficiency as high as 0.049 W/A. Lasing was achieved in spite of the large degree of resistive heating in the p-DBR, which was possible because of the high thermal conductivity of the binary GaAs/AlAs mirror layers and the small active area formed by the oxide aperture. This heating limited the maximum CW output power to 0.08 mW. Figure 4 shows emission spectra for a 5  $\mu\text{m}$  device at threshold, with a lasing wavelength of 1201.54 nm, and at 2.6 times threshold. The device lased in a single transverse and longitudinal mode, and far above threshold, the side mode suppression ratio was in excess of 40 dB. The wavelength shifted with dissipated power at 0.0924 nm/mW. Since broad area pulsed devices shifted at a rate of 0.0743 nm/K [4], this indicates a calculated temperature rise of  $\sim 60\text{K}$  above the ambient at peak output power.

In summary, we have demonstrated low-threshold GaInNAs VCSELs operating continuous-wave at room temperature with an emission wavelength of 1.2  $\mu\text{m}$ . Higher output power will be possible by reducing the resistance of the p-DBR, and we are presently working to achieve 1.3  $\mu\text{m}$  emission by increasing the indium and nitrogen content of the GaInNAs/GaAs multiple quantum well active layer. This work was performed under the auspices of the U.S. Department of Energy by University of California Lawrence Livermore National Laboratory under contract No. W-7405-Eng-48.

- [1] M. Kondow, et al., IEEE J. Selected Topics in Quantum Electronics 3, pp.719-730, 1997.  
 [2] M.C. Larson, et al., IEEE Photon. Technol. Lett. 10, pp. 188-190, 1998.  
 [3] C.W. Coldren, M.C. Larson, S.G. Spruytte, J.S. Harris, Electron. Lett., in press, 2000.  
 [4] C.W. Coldren, M.C. Larson, S.G. Spruytte, H.E. Garrett, J.S. Harris, CLEO '00, 2000.

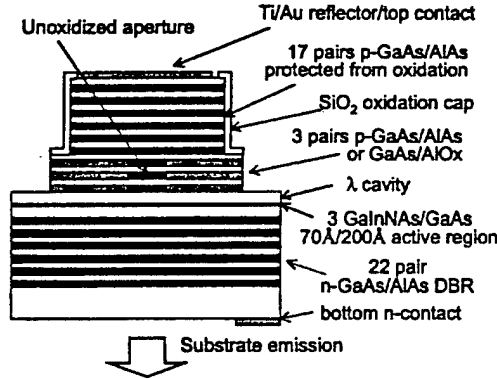


Fig. 1. Schematic diagram of GaInNAs vertical cavity laser.

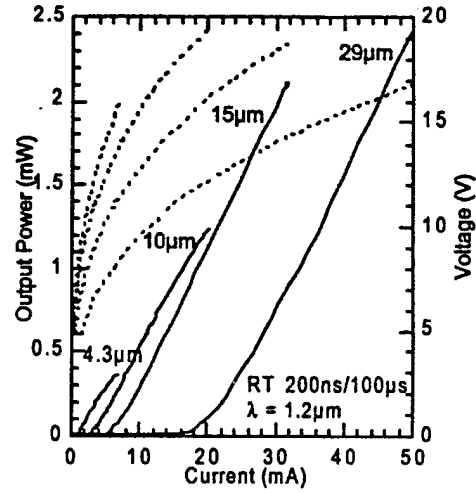


Fig. 2. Light output power (solid) and voltage (dotted) vs. injection current under pulsed operation.

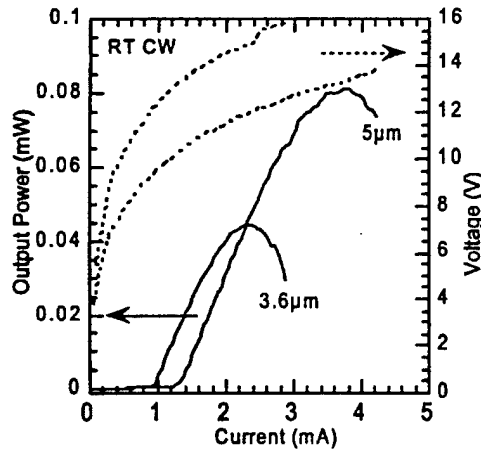


Fig. 3. Light output power (solid) and voltage (dotted) vs. injection current under CW operation.

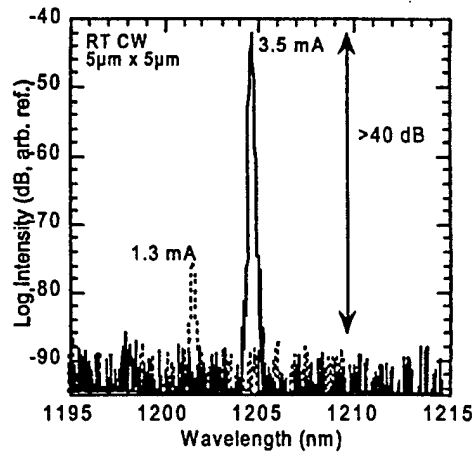


Fig. 4. Emission spectra at 1.3 mA ( $\sim I_{th}$ ) and 3.5 mA ( $\sim 2.6 I_{th}$ ).

# Group III nitride–arsenide long wavelength lasers grown by elemental source molecular beam epitaxy\*

C. W. Coldren,<sup>a)</sup> S. G. Spruytte, and J. S. Harris

*Solid State and Photonics Laboratory, Stanford University, Via Ortega, Stanford, California 94305*

M. C. Larson

*Lawrence Livermore National Laboratory, Livermore, California 94550*

(Received 10 October 1999; accepted 15 February 2000)

Elemental source molecular beam epitaxy was used to grow InGaAs quantum well samples, edge-emitting laser diodes, and vertical-cavity laser diodes on GaAs substrates. The quantum well samples exhibited an as-grown room temperature photoluminescence peak beyond 1310 nm which both increased dramatically in intensity and blueshifted with thermal annealing. Edge emitting laser diodes had threshold current densities as low as 450 and 750 A/cm<sup>2</sup> for single and triple quantum well active regions, respectively, and emitted light at 1220–1250 nm. The vertical cavity laser diodes emitted light at 1200 nm and had threshold current densities of 3 kA/cm<sup>2</sup> and efficiencies of 0.066 W/A. © 2000 American Vacuum Society. [S0734-211X(00)09603-7]

## I. INTRODUCTION

GaAs based vertical cavity surface emitting laser (VCSEL) diodes are becoming increasingly important in transmitters for high performance data links due to their low cost and ease of fiber coupling. However, the relatively short wavelength of conventional GaAs based VCSELs (820 nm) limits performance due to the wavelength dependent dispersion and loss properties of silica fiber. Additionally, the short wavelength limits the permissible optical power because of eye safety considerations. Longer optical wavelengths can overcome many of these limitations and allow data transmission at higher rates over longer distances.

The longest wavelengths achievable for devices on GaAs substrates have been typically around 1000 nm using InGaAs quantum wells. It is difficult to grow InGaAs quantum wells on GaAs with optical transitions beyond 1100 nm because increasing the indium content further leads to the formation of crystalline defects. Also, the addition to more indium to the quantum well material, in an attempt to achieve longer wavelengths, is a limited approach because both the strain energy and the quantum confinement energy increase with increasing indium content. The quantum confinement energy increases because increasing indium results in smaller effective masses and a deeper quantum wells (potentials) which both serve to push the first quantum confined level to higher energies. Much of the decrease in the bulk energy gap associated with increasing the indium content of the quantum well material is negated and more indium is required to achieve a given wavelength than would be predicted by the bulk band gap dependence on the indium mole fraction. Approaches to overcome these materials issues include InGaAs quantum dots,<sup>1</sup> GaAsSb quantum wells,<sup>2,3</sup> and InGaAs quantum wells.

The addition of nitrogen to InGaAs quantum wells results in the longest wavelengths achievable on GaAs substrates.

The role of nitrogen is twofold, the nitrogen causes the bulk band gap to decrease dramatically and second, the smaller lattice constant of GaN results in less strain in InGaAs compared to InGaAs by itself. Lasers beyond 1.3  $\mu\text{m}$  have been demonstrated with InGaAs active regions grown on GaAs substrates.<sup>4,5</sup> Previous reports of electrically injected InGaAs VCSELs have been limited to one structure employing a single quantum well active region emitting at 1180 nm.<sup>6</sup> We report the fabrication of both broad-area edge-emitting lasers and long wavelength VCSELs on GaAs substrates employing InGaAs single and multiple quantum well active regions with low threshold current densities.

## II. QUANTUM WELL SAMPLES

Growth was performed by elemental source molecular beam epitaxy where group III fluxes are provided by thermal effusion cells, dimeric arsenic is provided by a thermal cracker, and reactive nitrogen is provided by a rf plasma cell. The plasma cell is operated at 250–350 W with a gas flow of 0.1–0.5 sccm. Typical growth rates are 0.5–1  $\mu\text{m/h}$  for nitride–arsenide materials. The alloy contents of the grown layers were determined by both x-ray diffraction and secondary ion mass spectroscopy.

The quantum well samples were grown on Si-doped  $n^+$  GaAs substrates and consisted of two 70 Å  $\text{In}_{0.3}\text{Ga}_{0.7}\text{N}_{0.02}\text{As}_{0.98}$  quantum wells separated by 200 Å of GaAs. The growth temperature of the quantum wells was 440 °C. The room temperature photoluminescence spectrum for a quantum well sample as grown is shown in Fig. 1; also included is the spectrum for a sample that has undergone thermal annealing. Thermal annealing dramatically affects the luminescence of the quantum well materials, as the intensity can increase by an order of magnitude and the peak wavelength blueshifts significantly. Other groups have reported similar results.<sup>7</sup> The as-grown photoluminescence peak is at 1320 nm but shifts to 1230 nm with thermal annealing (with a substantial increase in intensity). The in-

\*No proof corrections received from author prior to publication.

<sup>a)</sup>Electronic mail: cwc@snw.stanford.edu

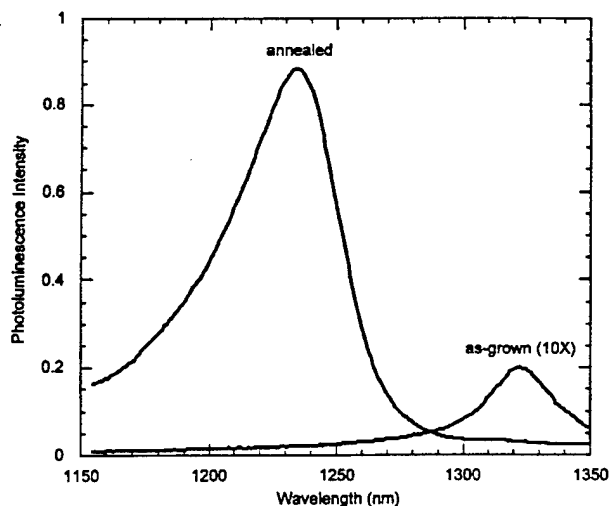


FIG. 1. Room temperature photoluminescence spectra of 70 Å InGaAs/GaAs quantum wells. Excitation was from the 514 nm line of an Ar<sup>+</sup> ion laser. The longer wavelength, lower intensity spectrum is for material as grown. The higher intensity spectrum at shorter wavelengths is for the same material that has been rapid thermal annealed at 740 °C for 60 s.

crease in intensity is presumably due to both the out diffusion of point defects and an increase in the crystalline quality of the quantum well material. The wavelength shift may be due to both nitrogen out diffusion and group III interdiffusion which could be more significant for InGaAs layers than for InGaAs layers under similar conditions due to possible elevated point defect densities associated with the growth of nitride-arsenide materials. Shown in Fig. 2 is the temperature dependence of the photoluminescence intensity and wavelength shift for proximity capped samples annealed for 60 s in a nitrogen ambient. The intensity increases dramatically after about 700 °C. The wavelength begins to shift rapidly at a lower temperature of about 660 °C. The decrease

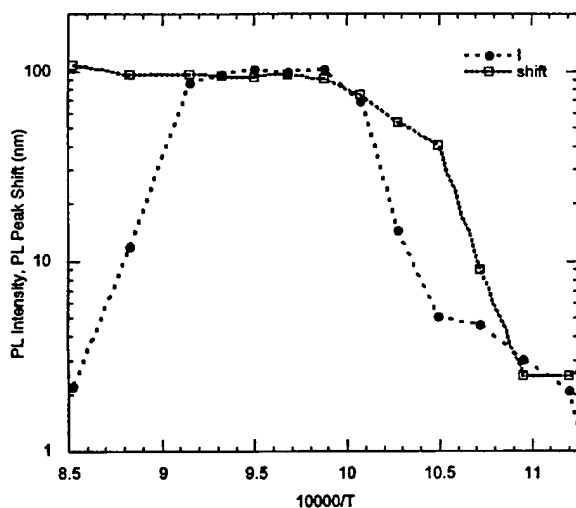


FIG. 2. Anneal temperature dependence of the photoluminescence intensity and wavelength shift. Samples were proximity capped and annealed for 60 s for temperatures in the range of 600–850 °C in a nitrogen ambient.

in photoluminescence intensity after about 790 °C is most likely due to the surface of the sample becoming deficient in arsenic.

### III. EDGE-EMITTING LASER DIODES

The layer structure of the fabricated edge-emitter lasers consisted of 1.7 μm of Al<sub>0.33</sub>Ga<sub>0.67</sub>As *n*-doped with Si at a level of  $1 \times 10^{18} \text{ cm}^{-3}$ , 100 nm GaAs, InGaAs/GaAs quantum well active region, 100 nm GaAs, 1.5 μm Al<sub>0.33</sub>Ga<sub>0.67</sub>As *p*-doped with Be at  $5 \times 10^{17} \text{ cm}^{-3}$ . A final 10 nm GaAs layer was grown with heavy *p* doping to facilitate electrical contact formation. The active regions consisted of either one or three InGaAs/GaAs quantum wells. The quantum well thickness was varied within the range of 65–90 Å in different samples. For the triple quantum well active regions, the quantum wells were separated by 200 Å of GaAs. The lower waveguide cladding layer was grown at 600 °C, the active regions at 420–460 °C, and the upper waveguide cladding layer in the range of 580–680 °C. Gold stripes 20 μm in diameter were fabricated by standard techniques and acted as the etch mask for the removal of the heavily doped contact layer. The stripe chips were cleaved into bars for testing.

The properties of the lasers depended strongly on the growth temperatures of the active region and the upper waveguide cladding. Optimized growth conditions yielded laser threshold current densities (for 20 μm wide by 800 μm long devices) as low as 450 and 600 A/cm<sup>2</sup> for single and triple quantum well active regions, respectively. The laser emission wavelengths were in the range of 1230–1250 nm.

The laser thresholds decreased as the growth temperature of the active region increased from 420 to 440 °C. Beyond 440 °C the threshold currents became higher as well as dependent on quantum well thickness. The trend in the quality of the reflection high-energy electron diffraction patterns seemed to follow the trend of the laser threshold currents. Most likely, the growth front becomes rougher and defects are generated at thinner well thickness as the temperature increases beyond 440 °C.

The high temperature growth of the upper waveguide cladding anneals the active region and therefore has a dramatic affect on laser performance. Laser threshold continued to decrease as the cladding growth temperature was increased. The maximum substrate temperature employed for the upper waveguide cladding was approximately 680 °C and yielded the lowest threshold lasers. The operating wavelengths of the lasers (the peak gain wavelength) also depended on the growth temperature of the upper cladding. For a cladding growth temperature of 600 °C, the laser wavelengths were around 1250 nm while a cladding growth temperature of 680 °C yielded wavelengths closer to 1230 nm. As detailed in the discussion of the quantum well photoluminescence above, the shift in the wavelengths (from the as-grown wavelength of 1320 nm) is most likely due to out diffusion of nitrogen and enhanced group III interdiffusion associated with elevated point defect densities occurring during nitride-arsenide growth. The photoluminescence inten-

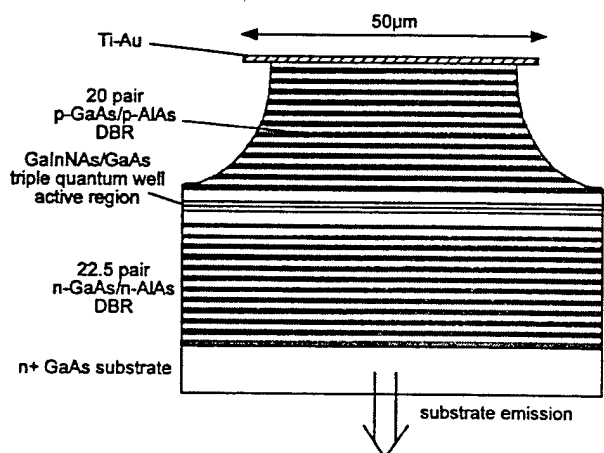


FIG. 3. VCSEL device structure. The InGaNaS quantum wells were 70 Å wide with 200 Å GaAs barriers. The active region was embedded in a one lambda long cavity.

sity had the largest increase in intensity for temperatures above 700 °C explaining the need for the high growth temperatures during the growth of the cladding.

#### IV. VCSEL DEVICES

A schematic of the VCSEL device structure is presented in Fig. 3. The VCSEL devices were designed for substrate emission at 1230 nm. The lower Si doped mirror consisted of 22.5 pairs of GaAs/AlAs quarter wave layers with electron concentrations of  $2 \times 10^{18} \text{ cm}^{-3}$ . The substrate temperature for the growth of the lower DBR was 600 °C. The active region was embedded in a one wavelength long cavity and consisted of three 70 Å InGaNaS quantum wells separated by 200 Å of GaAs all grown at 440 °C. The upper Be doped mirror consisted of 20 pairs of AlAs/GaAs quarter wave layers with hole concentrations of  $5 \times 10^{17} \text{ cm}^{-3}$  for the first ten periods and then  $1 \times 10^{18} \text{ cm}^{-3}$  for the final ten periods. To minimize the resistance associated with the large number of heterojunctions, the Be doping was modified and the alloy content was graded over a distance of 180 Å between the DBR mirror layers. The Be doping was eliminated on the narrow band gap side of the graded regions and was increased to yield hole concentrations of  $2 \times 10^{18} \text{ cm}^{-3}$  on the wide band gap sides. The upper DBR mirror was grown at approximately 660 °C. Ti/Au pads 50 μm in diameter were formed by evaporation and liftoff to both increase the reflectivity of the top mirror and to make electrical contact to the *p* region of the diodes. Electrical contact was made to the *n* region of the diodes through the backside of the substrate. Wet chemical etching defined mesas to minimize current spreading.

The device properties were measured at room temperature without heat sinking using 200 ns current pulses at a 10 kHz repetition rate. The vertical cavity laser emission spectrum, with the device driven just above threshold, is shown in Fig. 4. The optical output power versus drive current characteristics for the 50 μm × 50 μm device are shown in Fig. 5. The

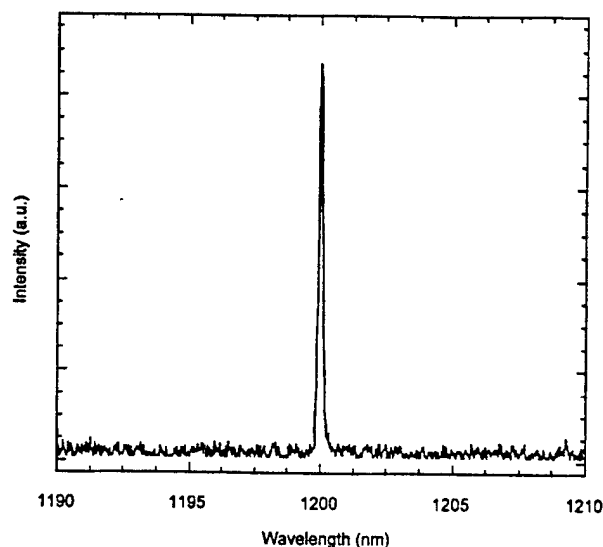


FIG. 4. Laser emission spectrum for InGaNaS VCSEL device. The device was biased just above threshold.

laser threshold current was as low as 66 mA or 2.6 kA/cm<sup>2</sup>. The slope efficiency was measured to be 0.066 W/A. The threshold voltage was approximately 12 V. The soft turn on may be due to optical interference effects associated with the reflections from the backside of the substrate. Also seen in Fig. 5, high total output powers were obtained. Thickness nonuniformity across the wafer also resulted in lasers emitting at wavelengths as long as 1210 nm.

Based on the performance of the optimized edge emitters described earlier, the VCSEL design should have yielded threshold current densities of 1–2 kA/cm<sup>2</sup>. The higher threshold currents for the fabricated devices are most likely due to higher optical losses than expected and a slightly

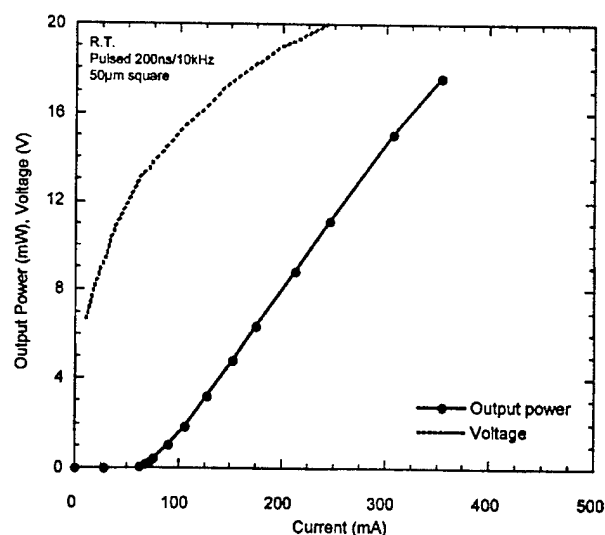


FIG. 5. VCSEL output power and voltage vs current measured using 200 ns current pulses at a 10 kHz repetition rate. Measurements were performed at room temperature without any heatsinking.

lower *in situ* anneal temperature, i.e., the growth temperature for the upper DBR mirror. The top DBR was grown at a sufficiently high temperature that gallium desorption became significant and resulted in thinner than desired GaAs layers. The thinner GaAs layers resulted in a reduced reflectivity and a shift in the resonance wavelength of the devices from the design wavelength of 1230 nm to a measured wavelength of 1200 nm. As evidenced by the high voltages, the high temperature growth also resulted in a smearing out of the Be doping profile that was designed to reduce the resistance of the top *p*-type DBR. The loss of the designed doping profile can also affect the optical losses, as highly absorbing hole accumulation layers can develop on the GaAs side of the GaAs/AlAs heterojunctions. Furthermore, the long growth time (12 h) at high temperature for the top DBR resulted in a significant blueshift of the quantum well luminescence spectrum (and therefore the gain spectrum) relative to that of the edge-emitter lasers.

Compared with previous nitride-arsenide VCSEL results,<sup>6</sup> the optimized active region with higher nitrogen content results in a lower threshold current, longer wavelength, and a higher efficiency.

## V. CONCLUSION

VCSEL based transmitters operating at wavelengths longer than the current ( $<1\ \mu\text{m}$ ) GaAs based devices will enable higher performance data links and lower cost optical

communications systems. Elemental source molecular beam epitaxy was used to grow InGaAs laser active region and device structures with emission wavelengths beyond  $1.2\ \mu\text{m}$ . Edge-emitter lasers based on InGaAs active regions had threshold current densities as low as  $450\ \text{A}/\text{cm}^2$  and wavelengths as long as  $1.25\ \mu\text{m}$ . Finally, GaAs based VCSEL devices employing three InGaAs quantum wells were fabricated had resulted in laser emission at a wavelength of  $1.2\ \mu\text{m}$ . The VCSEL devices had threshold current densities of  $2.6\ \text{kA}/\text{cm}^2$  and efficiencies of  $0.066\ \text{W}/\text{A}$ .

## ACKNOWLEDGMENTS

This research was supported by DARPA and the DOE.

<sup>1</sup>D. L. Huffaker, J. D. Schaub, D. Hongyu, and D. G. Deppe, *Proc. SPIE* **3283**, 144 (1998).

<sup>2</sup>T. Anan, K. Nishi, S. Sugou, M. Yamada, K. Tokutome, and A. Gomyo, *Electron. Lett.* **34**, 2127 (1998).

<sup>3</sup>M. Yamada, T. Anan, K. Tokutome, K. Nishi, A. Gomyo, and S. Sugou, *Conference Proceedings LEOS'98*, pp. 149–50.

<sup>4</sup>K. Nakahara, M. Kondow, T. Kitatani, M. C. Larson, and K. Uomi, *IEEE Photonics Technol. Lett.* **10**, 487 (1998).

<sup>5</sup>F. Hohnsdorf, J. Koch, S. Leu, W. Stolz, B. Borchert, and M. Druminski, *Electron. Lett.* **35**, 571 (1999).

<sup>6</sup>M. C. Larson, M. Kondow, T. Kitatani, K. Nakahara, K. Tamura, H. Inoue, and K. Uomi, *IEEE Photonics Technol. Lett.* **10**, 188 (1998).

<sup>7</sup>H. P. Xin, K. L. Kavanagh, M. Kondow, and C. W. Tu, *International Molecular Beam Epitaxy Conference, Cannes, France [J. Cryst. Growth* **201–202**, 419 (1998)].

## References

- 1 NAYAR, S.K., SANDERSON, A.C., WEISS, L.E., and SIMON, D.D.: 'Specular surface inspection using structured highlight and Gaussian images', *IEEE Trans. Robot. Autom.*, 1990, 6, (2), pp. 208-218
- 2 KIM, T.H., CHO, T.H., MOON, Y.S., and PARK, S.H.: 'Visual inspection system for the classification of solder joints', *Patt. Recogn.*, 1999, 32, pp. 565-575
- 3 HAYKIN, S.: 'Neural network: a comprehensive foundation' (Prentice Hall, 1999), 2nd edn.
- 4 SCHOLKOFF, B., SUNG, K., BURGESS, C., GIROSI, F., NIYOGI, P., POGIO, T., and VAPNIK, V.: 'Comparing support vector machines with Gaussian kernels to radial basis function classifiers'. A.I. Memo 1599

## 1200nm GaAs-based vertical cavity lasers employing GaInNAs multiquantum well active regions

C.W. Coldren, M.C. Larson, S.G. Spruytte and J.S. Harris

Elemental source molecular beam epitaxy has been used to grow vertical cavity laser diodes on GaAs substrates that employ GaInNAs multiquantum well active regions and AlAs/GaAs distributed Bragg reflectors. The laser diodes emitted light at 1200nm and had threshold current densities of 2.5kA/cm<sup>2</sup> and efficiencies of 0.066W/A under room temperature pulsed operation.

**Introduction:** GaAs-based vertical cavity surface emitting laser (VCSEL) diodes are becoming increasingly important in transmitters for high performance optical fibre data links due to their low cost and ease of fibre coupling. However, the relatively short (850nm) wavelengths of conventional GaAs based VCSELs can limit performance due to the wavelength-dependent dispersion and loss properties of silica fibre. GaInNAs active regions grown on GaAs substrates have enabled the realisation of in-plane laser diodes emitting beyond 1300nm where fibre performance is more optimal [1, 2]. Previous reports of GaInNAs vertical cavity laser diodes have been limited to one structure employing a single quantum well active region emitting at 1180nm [3].

We report the fabrication of broad area long wavelength VCSELs on GaAs substrates employing a GaInNAs triple quantum well active region. The higher gain available from this active region allows for lowered mirror reflectivity requirements and a correspondingly higher efficiency. VCSELs with an emission wavelength of 1200nm exhibited threshold current densities of 2.5kA/cm<sup>2</sup> and slope efficiencies of 0.066W/A under pulsed room temperature operation.

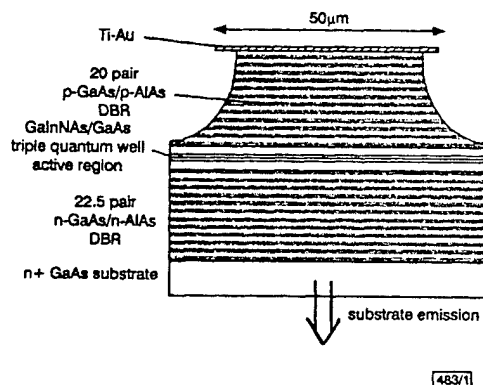


Fig. 1 GaInNAs VCSEL device structure

**Device fabrication:** A schematic diagram of the VCSEL device structure is presented in Fig. 1. The device was designed for substrate emission at a wavelength of 1.23µm and was grown by elemental source molecular beam epitaxy using an arsenic cracker

and a nitrogen RF plasma cell. The lower *n*-type mirror consisted of 22.5 pairs of GaAs/AlAs quarter wave layers doped with Si at a level of  $2 \times 10^{18}$ cm<sup>-3</sup> and grown at a substrate temperature of 600°C. The active region, consisting of three 70Å GaInNAs quantum wells separated by 200Å GaAs barriers all grown at 440°C, was embedded in a 1λ cavity. The upper *p*-type mirror consisted of 20 pairs of AlAs/GaAs quarter wave layers doped with Be at  $5 \times 10^{17}$ cm<sup>-3</sup> for the first 10 periods and then  $10^{18}$ cm<sup>-3</sup> for the final 10 periods. To minimise the resistance associated with the heterojunctions, the alloy content was graded over a distance of 180Å and the doping levels were increased to  $2 \times 10^{18}$ cm<sup>-3</sup> on the wide bandgap side of the heterojunction grading regions and the doping was eliminated on the narrow bandgap side. Square 50 × 50µm Ti/Au pads were formed by evaporation and lift-off to both increase the reflectivity of the top mirror and make electrical contact to the *p*-region of the diode. Electrical contact was made to the *n*-region of the diode through the backside of the substrate. Wet chemical etching was used to define mesas to minimise current spreading.

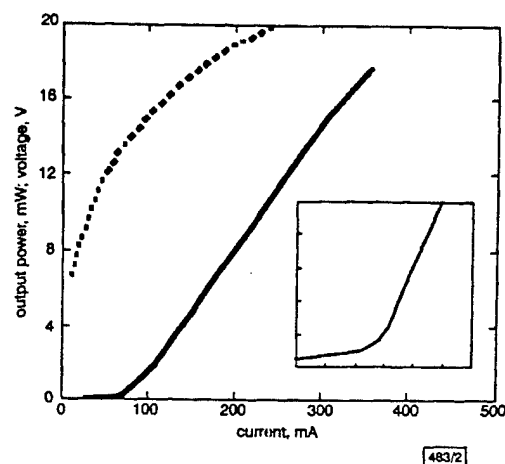


Fig. 2 Light output power and voltage against injection current (L-I-V) characteristics at room temperature for GaInNAs VCSEL

— output power  
--- voltage  
Inset: details of threshold region

**Device characteristics:** The device properties were measured at room temperature without heatsinking using 200ns current pulses at a 10kHz repetition rate. The output power against injection current is shown in Fig. 2. The laser threshold, as determined from the inset of Fig. 2, is 65mA, which corresponds to a threshold current density of 2.5kA/cm<sup>2</sup>. The slope efficiency, well above threshold, was 0.066W/A, and peak output power above 17mW was obtained. The threshold voltage was ~13V.

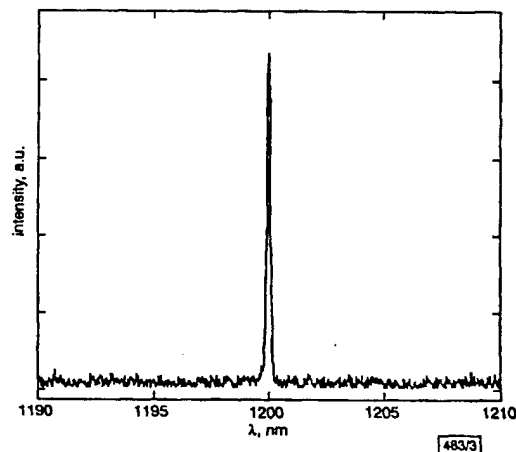


Fig. 3 GaInNAs VCSEL emission spectrum

The emission spectrum near lasing threshold is shown in Fig. 3. The spectrum is centred at 1200nm with a linewidth of  $< 0.2$ nm. Above threshold, the spectrum exhibited multiple peaks with approximately 0.4nm spacing and an envelope that broadened with current, which was probably a result of thermally-induced chirp during the current pulse in conjunction with optical feedback induced by the reflection from the substrate backside. Thickness nonuniformity across the wafer resulted in lasers emitting at wavelengths as long as 1215nm.

Another device with a less-reflective Ti/Pt/Au pad metallisation, but otherwise identical structure, was characterised for comparison. Here the slope efficiency was 0.029W/A and threshold current density was 4.8kA/cm<sup>2</sup>, indicating a roughly two-fold increase in the round-trip optical loss. However, the fact that laser oscillation was still achieved is indicative of the high gain of the active layer, implying considerable flexibility in designing optimised devices with lower bottom (output) mirror reflectivity for higher efficiency and higher mirror doping for lower operating voltage.

Edge emitting lasers employing similar GaInNAs quantum wells were also fabricated. The threshold current densities for 20 $\mu$ m wide and 800 $\mu$ m long stripe lasers were as low as 450 and 600A/cm<sup>2</sup> for single and triple quantum well active regions, respectively, and devices lased at wavelengths of 1230–1250nm. Based on the performance of these edge emitters the VCSEL design should have yielded threshold current densities of 1–2kA/cm<sup>2</sup>. Growth inaccuracy resulted in a shift of the wavelength of the devices from the design wavelength of 1230nm to 1200nm with increased optical loss. Additionally, the long duration (12h) growth of the top mirror at elevated temperature resulted in a significant shift in the luminescence spectrum of the quantum wells due most probably to atomic inter-diffusion between the quantum well and the barrier. These effects may explain the higher than expected threshold currents. Furthermore, the high voltages are most likely the result of the smearing out of the *p*-doping profile due to out-diffusion of Be from AlAs during growth.

**Conclusion:** VCSEL-based transmitters operating at wavelengths longer than the current  $< 1\mu$ m of GaAs-based devices will enable higher performance data links and optical interconnection systems. We reported a GaAs-based VCSEL that employs three GaInNAs quantum wells with an emission wavelength of 1200nm. The device has a threshold current density of 2.5kA/cm<sup>2</sup> and a slope efficiency of 0.066W/A.

**Acknowledgments:** This work was performed under the auspices of the Army Research Office and the US Department of Energy by Lawrence Livermore National Laboratory under contract W-7405-Eng-48.

© IEE 2000

28 March 2000

Electronics Letters Online No: 20000365

DOI: 10.1049/el:20000365

C.W. Coldren, S.G. Spruytte and J.S. Harris (Solid State and Photonics Laboratory, Stanford University, CIS 126X, Via Ortega, Stanford, CA 94305, USA)

M.C. Larson (Lawrence Livermore National Laboratory, PO Box 808, L-222, Livermore, CA 94551, USA)

C.W. Coldren: Also with Lawrence Livermore National Laboratory, PO Box 808, L-222, Livermore, CA 94551, USA

## References

- 1 NAKAHARA, K., KONDOW, M., KITATANI, T., LARSON, M.C., and UOMI, K.: '1.3- $\mu$ m continuous-wave lasing operation in GaInNAs quantum-well lasers', *IEEE Photonics Technol. Lett.*, 1998, 10, (4), pp. 487–488
- 2 SATO, S., OSAWA, Y., SAITOH, T., and FUJIMURA, I.: 'Room temperature pulsed operation of 1.3 $\mu$ m GaInNAs/GaAs laser diode', *Electron. Lett.*, 1997, 33, (16), pp. 1386–1387
- 3 LARSON, M.C., KONDOW, M., KITATANI, T., NAKAHARA, K., TAMURA, K., INOUE, H., and UOMI, K.: 'GaInNAs-GaAs long-wavelength vertical-cavity surface-emitting laser diodes', *IEEE Photonics Technol. Lett.*, 1998, 10, (2), pp. 188–190

## Demonstration of passive Q-switching in multiquantum well InGaAs/AlGaInAs diode laser

V. Loyo-Maldonado, S.D. McDougall, J.H. Marsh, J.S. Aitchison and C.C. Button

The first passive Q-switched operation is reported of an InGaAs/AlGaInAs diode laser with a frequency repetition ranging from 1 to 2.5GHz at the emitting wavelength of 1.58 $\mu$ m. This material is important as a thermally stable alternative to InGaAsP based laser systems operating around 1.5 $\mu$ m.

**Introduction:** Recently the search for improved performance and thermal stability of long wavelength semiconductor lasers (operating around 1.5 $\mu$ m) has led to increasing interest in the InGaAs/AlGaInAs quantum well material system as an alternative to InGaAsP. Al-quaternary systems and P-quaternary systems have many similar properties such as the range of bandgaps (i.e. emitting wavelengths), carrier mobility and refractive index. However, an important difference exists between them: Al-quaternary material has a larger conduction band offset ( $\Delta E_c/\Delta E_g$ ) [1]. Owing to the larger conduction band offsets in the InGaAs/AlGaInAs system ( $\Delta E_c/\Delta E_g = 0.7$ ) compared to InGaAsP ( $\Delta E_c/\Delta E_g = 0.4$ ), electron confinement in the quantum well can remain strong with increasing temperature, allowing lasers to be operated without cooling. Some recent publications have shown [2–4] that, in applications where high temperature operation is especially important, Al-quaternary lasers are expected to perform better than those fabricated in P-quaternary systems.

Q-switched lasers find applications in communication and sensing systems where a short pulse source with a controllable repetition rate is required. The width of the pulse from a Q-switched laser is typically of the order of 10–100ps, depending on the length of the cavity. Q-switched semiconductor lasers are always multi-section diodes and they must have at least one absorber section (introducing saturable loss into the cavity) and one gain section. In multiquantum well (MQW) material, a reverse bias section can be used as a saturable absorber which can then either passively Q-switch, or mode-lock the laser depending on the relative length of the gain and absorber section. In this Letter, we report the first demonstration to our knowledge of passive Q-switching in an MQW two-section InGaAs/AlGaInAs laser diode emitting at 1.582 $\mu$ m.

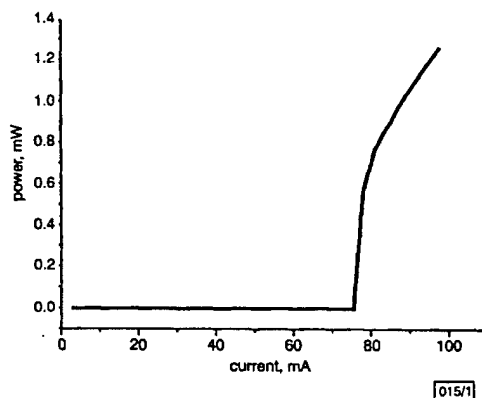


Fig. 1 Light-current characteristic of two-section InGaAs/AlGaInAs laser

The two different slopes follow the 'snap-on' behaviour due to the presence of the saturable absorber in the cavity

**Material system:** The material used to fabricate the devices consists of six pairs of 7nm InGaAs wells sandwiched by 8nm Al<sub>0.2</sub>Ga<sub>0.77</sub>In<sub>0.53</sub>As barriers. The *p*-doped upper cladding consists of a 1.5 $\mu$ m layer of AlInAs with a *p*<sup>+</sup> contact layer of 200nm InGaAs on top. The *n*-doped lower cladding consists of a 500nm layer of AlInAs grown on top of a 600nm layer of InP (buffer). The whole structure has been grown lattice matched (*x+y* = 0.47) to an InP substrate. The electron confinement energy in the well

# Electrical depth profile of *p*-type GaAs/Ga(As,N)/GaAs heterostructures determined by capacitance–voltage measurements

P. Krispin<sup>a)</sup>

*Paul-Drude-Institut für Festkörperelektronik, Hausvogteiplatz 5-7, 10117 Berlin, Germany*

S. G. Spruytte and J. S. Harris

*Solid State and Photonics Laboratory, Stanford University, Stanford, California 94305*

K. H. Ploog

*Paul-Drude-Institut für Festkörperelektronik, Hausvogteiplatz 5-7, 10117 Berlin, Germany*

(Received 1 May 2000; accepted for publication 5 July 2000)

Capacitance–voltage measurements on metal–semiconductor contacts are used to examine depth-resolved electrical characteristics of GaAs/Ga(As,N)/GaAs heterostructures. The experimental depth profiles of the carrier concentration are compared with calculations based on self-consistent solutions of the Poisson equation. As-grown Ga(As,N) layers are *p* type, and hole concentrations of about  $3 \times 10^{16} \text{ cm}^{-3}$  are observed for undoped Ga(As,N) layers with a GaN mole fraction of 3% and thicknesses below 80 nm. This hole concentration is stable during rapid thermal annealing. For a GaN mole fraction of about 3%, the valence band offset between GaAs and Ga(As,N) is found to be  $+(11 \pm 2) \text{ meV}$ . The heterointerfaces are of type I. The dominant carrier depletion in as-grown heterostructures is due to donor-like defect levels, which are accumulated at the GaAs-on-Ga(As,N) interface. The amount of these interfacial defects rises remarkably in thicker Ga(As,N) layers, but can be completely removed by rapid thermal annealing after growth. By release spectroscopy, further hole traps with definite level energies are distinguished at the Ga(As,N)-on-GaAs interface, which are probably due to the specific GaAs growth conditions.

© 2000 American Institute of Physics. [S0021-8979(00)00220-6]

## I. INTRODUCTION

Group III arsenide nitrides grown on GaAs substrates are promising materials with a wide range of potential applications in optoelectronic devices,<sup>1–4</sup> particularly, in vertical-cavity surface-emitting laser diodes<sup>5–7</sup> and solar cells.<sup>8</sup> Ga(As,N) layers are of special interest, because the introduction of small amounts of nitrogen into GaAs has a remarkable effect on electronic properties. In particular, the band gap is drastically reduced.<sup>9–11</sup> Until now, the electronic properties of Ga(As,N) have been mainly investigated by optical techniques,<sup>9,12–19</sup> but often on layers with thicknesses above  $1 \mu\text{m}$ .<sup>14,18,19</sup> In the latter case, the results are related to the relaxed Ga(As,N) lattice, and not to Ga(As,N) layers with coherent tensile strain. The electrical characteristics of strained Ga(As,N) layers are practically unknown. Moreover, there is no information available about the electronic perfection of the normal [Ga(As,N)-on-GaAs] and inverted [GaAs-on-Ga(As,N)] interfaces, although the interfaces between semiconducting layers become increasingly important in low-dimensional structures.

The band discontinuities between Ga(As,N) and GaAs are discussed. In particular, type II heterointerfaces were inferred from x-ray photoelectron spectroscopic studies,<sup>20</sup> in agreement with theoretical calculations from a dielectric model.<sup>21</sup> Type I heterointerfaces were predicted by first principle calculations.<sup>22</sup> It should be noted that the experimental data in Ref. 20 could also be associated with type I character, because the limited energy resolution leads to

extremely large errors for the valence band offset  $\Delta E_V$ .

It is known that the band offset can be determined very accurately by capacitance versus voltage (*C–V*) measurements.<sup>23,24</sup> Moreover, the *C–V* technique provides information on carrier distributions and interfacial defect levels.<sup>23–26</sup> Therefore we use *C–V* measurements on rectifying metal–semiconductor (MS) contacts on *p*-type GaAs/Ga(As,N)/GaAs heterostructures grown by molecular beam epitaxy (MBE) to examine the depth-resolved electrical characteristics. The experimental depth profiles of the carrier concentration are compared with calculations based on self-consistent solutions of the Poisson equation. In particular, coherently strained Ga(As,N) layers are studied with a GaN mole fraction of about 3%.

The valence band offset between GaAs and GaAs<sub>0.97</sub>N<sub>0.03</sub> is found to be  $+(11 \pm 2) \text{ meV}$ . Hence, type I heterointerfaces are established. Due to the high depth resolution, the two interfaces of the isotype heterojunctions can be discriminated. We show that the dominant carrier depletion in as-grown heterostructures is not caused by compensating defects in the Ga(As,N) layer. The large carrier deficit is associated with donor-like defect levels, which are accumulated at the GaAs-on-Ga(As,N) interface. It is experimentally verified that the amount of these interfacial defects can be completely removed by rapid thermal annealing after growth.

## II. EXPERIMENTAL DETAILS

The investigated GaAs/Ga(As,N)/GaAs heterostructures were grown by elemental source MBE on *p*<sup>+</sup>-type

<sup>a)</sup>Electronic mail: krispin@pdi-berlin.de

GaAs(001) substrates. Dimeric arsenic and atomic nitrogen were provided by a thermal cracker and a radio frequency (rf) nitrogen plasma cell, respectively. Details of the growth are published elsewhere.<sup>27</sup> The layer structure consisted of about 1  $\mu\text{m}$  Be-doped GaAs grown at 620  $^{\circ}\text{C}$ , the Ga(As, N) layer grown at 500  $^{\circ}\text{C}$ , and approximately 200 nm Be-doped GaAs grown at 620  $^{\circ}\text{C}$  on top. The hole concentration in GaAs as determined by the  $C$ - $V$  method was about  $3 \times 10^{16} \text{ cm}^{-3}$ . Changes of the growth temperature took 2 min and were performed during GaAs growth. The GaAs region, in which the growth temperature was gradually changed, was about 15 nm thick. The GaN mole fraction was 3% as determined from high resolution x-ray diffraction (HRXRD) measurements and secondary ion mass spectrometry (SIMS). The thickness of the Ga(As, N) layers varied between 10 and 70 nm. We observed no strain relaxation as checked by HRXRD. Rapid thermal annealing was performed for 60 s at 760  $^{\circ}\text{C}$  with a GaAs proximity cap under  $\text{N}_2$  atmosphere in order to check, which of the growth-related defects can be removed.

Ohmic contacts were realized with Au/Be on the  $p^+$ -type GaAs substrate. The MS contacts for the electrical measurements were formed by vacuum-deposited Ti/Au dots on the GaAs top layer. The capacitance and ac conductance were measured at 80 and 300 K with an HP LCR meter 4275 A in the frequency range from 10 kHz to 2 MHz. The loss factor was kept below 0.1.

The depth profile of the apparent free hole concentration  $N_{C-V}$  was measured using the conventional  $C$ - $V$  method.<sup>24</sup> The concentration  $N_{C-V}$  was obtained from the expression

$$N_{C-V}(W) = \frac{2}{A^2 q \epsilon \epsilon_0} \left[ \frac{d}{dV} \left( \frac{1}{C^2} \right) \right]^{-1}, \quad (1)$$

where  $W$  denotes the thickness of the space-charge layer below the MS contact,  $A$  the contact area,  $q$  the elementary charge, and  $\epsilon \epsilon_0$  the dielectric constant. In general,  $N_{C-V}$  is equal to the free hole density  $p$  at the edge of the space charge layer.<sup>24</sup> The depth  $W$  was calculated from the depletion capacitance  $C$  using

$$W(V) = \epsilon \epsilon_0 A / C(V). \quad (2)$$

For nondegenerate semiconductor structures, the spatial resolution of the carrier density versus depth profile is limited by the Debye screening length  $L_D = \sqrt{\epsilon \epsilon_0 kT / q^2 p}$ , where  $k$  denotes Boltzmann's constant and  $T$  the temperature. For a hole density  $p$  of  $3 \times 10^{16} \text{ cm}^{-3}$ , the  $L_D$  values are about 13 and 25 nm at 80 and 300 K, respectively. By changing a dc bias in reverse direction, the edge of the space charge layer below the contact could be shifted across the Ga(As, N) layer. According to the depth resolution limit of capacitance measurements, the two interfaces of isotype heterostructures can be distinguished by the  $C$ - $V$  method at 80 K for Ga(As, N) layers thicker than 30 nm. Because at lower temperatures the series resistance of the samples leads very often to a frequency dispersion above 100 kHz,<sup>24</sup> the depth profiles of the concentration  $N_{C-V}$  at 80 K were determined at 10

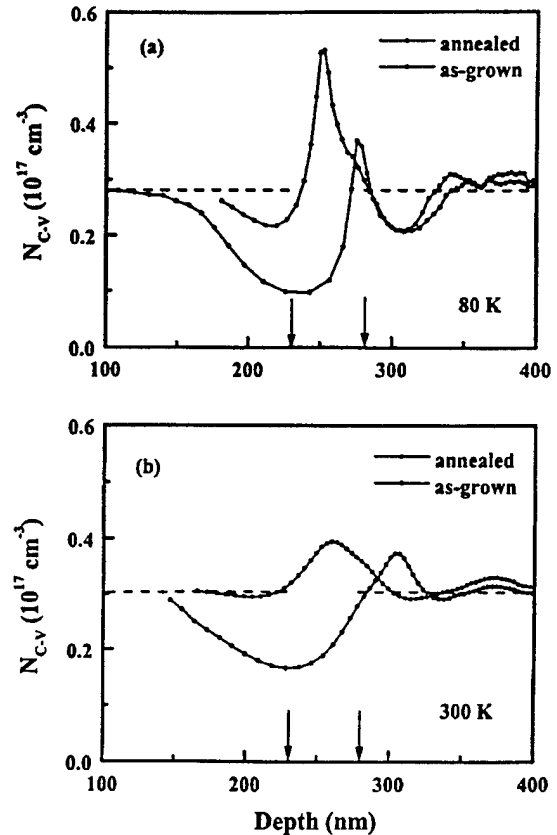


FIG. 1. Typical depth profiles of the apparent hole concentration  $N_{C-V}$  for sample No. 1 with 50 nm not-intentionally doped Ga(As, N) measured (a) at 80 K and 10 kHz and (b) at 300 K and 1 MHz with test voltages  $V_{ac} = kT/q$ . Dashed lines indicate the doping level of the GaAs layers. The interface positions are marked by arrows.

kHz. At 300 K, we found no frequency dependence of the capacitance up to 2 MHz.

Based on self-consistent solutions of the Poisson equation, one-dimensional simulations of the investigated heterojunctions were carried out, in order to determine the valence band offset  $\Delta E_V$ , the hole concentration in the Ga(As, N) layer, as well as the amount and character of fixed charges at the normal and inverted interfaces. The Poisson-Schrödinger solver of Snider *et al.*<sup>28</sup> was used to calculate capacitance versus voltage characteristics. The fit to measured capacitance values was generally better than 2% in relevant bias regions. The theoretical depth profiles of the apparent carrier density  $N_{C-V}$  were obtained from Eqs. (1) and (2). Standard GaAs values were used for the dielectric constant and the effective density of states. It should be noted that the calculations do not take into account interfacial traps, which loose their holes when the Fermi level crosses the trap levels with increasing reverse bias.<sup>24-26</sup> ac responses of deep states are also not considered by the above Schrödinger-Poisson solver.<sup>24</sup>

### III. RESULTS AND DISCUSSION

#### A. Evaluation of hole distribution

For an as-grown and annealed heterostructure with 50 nm not intentionally doped Ga(As, N) (sample No. 1), char-

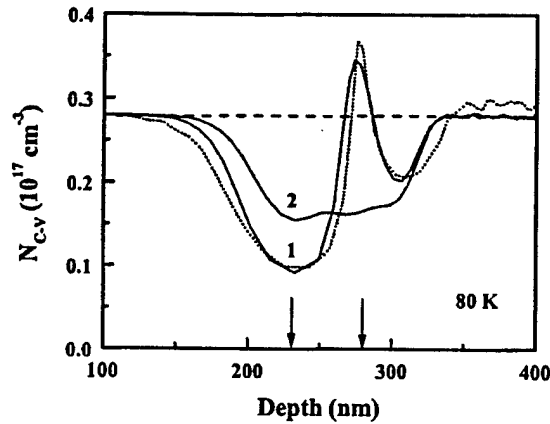


FIG. 2. Simulation of the carrier distribution measured at 80 K on the as-grown sample No. 1 [see Fig. 1(a)]. The experimental  $N_{C-V}$  vs depth profile (dotted line) is best fitted by curve 1, which was calculated with interface positions at 230 and 280 nm (indicated by arrows), a valence band offset of 13 meV, fixed charges of  $1.4 \times 10^{11} \text{ cm}^{-2}$  at the inverted interface, and a bulk hole concentration of  $2.8 \times 10^{16} \text{ cm}^{-3}$  in the Ga(As, N) layer. The doping level is marked by the dashed line. For the calculation of curve 2, holes in Ga(As, N) as well as fixed charges at the inverted interface were neglected.

acteristic depth profiles of the apparent hole concentration  $N_{C-V}$  are shown in Figs. 1(a) and 1(b) for temperatures of 80 and 300 K, respectively. Whereas the doping level of about  $3 \times 10^{16} \text{ cm}^{-3}$  is evident for the GaAs layers (dashed lines), the Ga(As, N) region (between the arrows) reveals a complex response, and the carrier density inside the Ga(As, N) layer cannot be determined directly. For the as-grown sample, we observe a distinct depletion at the GaAs-on-Ga(As, N) interface. The total carrier deficit is found to be about  $1.2 \times 10^{11} \text{ cm}^{-2}$  at 300 K. The peak-valley structure shown in Fig. 1(a) at about 290 nm is characteristic for an isotype heterointerface.<sup>23</sup> After annealing the sample, the carrier depletion at the inverted interface is drastically reduced, and the hole concentration is enhanced in the Ga(As, N) layer. Both GaAs regions adjacent to the Ga(As, N) layer are then depleted. This transfer of holes from the adjacent GaAs layers to the higher valence band edge of Ga(As, N) in conjunction with the smaller band gap of Ga(As, N) indicates the type I character of GaAs/Ga(As, N) interfaces. By comparing the two curves in Fig. 1(a), it is evident that the electrical characteristics of the Ga(As, N)-on-GaAs interface is stable under annealing.

More information about carrier concentration in the Ga(As, N) layer and interface charges is gained by comparing the measured carrier distributions in Fig. 1(a) with calculated depth profiles. Figure 2 shows the simulation of the carrier density in the as-grown sample No. 1 at 80 K. The best fit (curve 1 in Fig. 2) is obtained for a valence band offset  $\Delta E_V$  of 13 meV for both interfaces, no trapped charges at the normal interface,  $1.4 \times 10^{11} \text{ cm}^{-2}$  fixed positive charges at the inverted interface, and a hole density of  $2.8 \times 10^{16} \text{ cm}^{-3}$  in the Ga(As, N) layer. For the calculation of curve 2, holes in Ga(As, N) were neglected. By comparing curves 1 and 2 in Fig. 2, it is demonstrated that the carrier accumulation at the normal interface can be only understood,

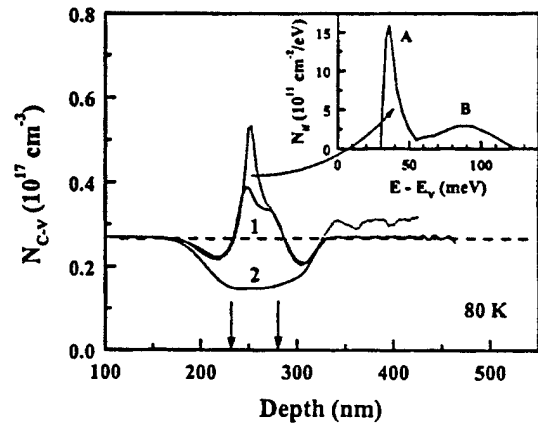


FIG. 3. Simulation of the carrier distribution measured at 80 K on the annealed sample No. 1 [see Fig. 1(a)]. The experimental  $N_{C-V}$  vs depth profile (dotted line) is best fitted by curve 1, which was calculated using interface positions at 230 and 280 nm (indicated by arrows), a valence band offset of 11 meV, no fixed interfacial charges, and a bulk hole concentration of  $2.7 \times 10^{16} \text{ cm}^{-3}$  in the Ga(As, N) layer. The doping level is marked by the dashed line. For the calculation of curve 2, holes in Ga(As, N) were neglected. In the inset, the release spectrum of the state density  $N_{if}$  is shown for the inverted interface after annealing. The responses of interfacial hole traps A and B are indicated.

if free holes in the Ga(As, N) layer are present. As-grown Ga(As, N) is *p*-type. As SIMS depth profiles showed the Ga(As, N) layer does not contain Be, the holes are due to impurities (like carbon) or intrinsic defects in the Ga(As, N) layer. The as-grown normal interface is obviously free of trapped carriers. The carrier depletion measured at 300 K for the as-grown sample No. 1 [see Fig. 1(b)] can be perfectly fitted with the same values for interface charges, hole concentrations, and valence band offset. Therefore, the dominant depletion in as-grown heterostructures is caused by fixed positive charges at the inverted interface and not by intrinsic or extrinsic hole traps in the Ga(As, N) layer.

For the annealed sample No. 1 (Fig. 1), results of the simulation are depicted in Fig. 3 for a temperature of 80 K. The best fit (curve 1) is achieved for a valence band offset  $\Delta E_V$  of 11 meV for both interfaces and the same hole concentration in annealed Ga(As, N) as in the as-grown material. In contrast to the as-grown heterostructure of Fig. 2, fixed charges at the inverted interface are no longer necessary to fit the experimental results, i.e., the trap levels at the inverted interface of the as-grown structure can be completely removed by annealing. The valleys characteristic for isotype heterojunctions are therefore developed at both interfaces on the GaAs sides.

## B. Energy distribution of interfacial hole traps

At first sight, the sharp peak apparent at 250 nm in the measured hole distribution (dotted line in Fig. 3) looks like a delta-doped layer inside annealed Ga(As, N). But our simulations show that a peak related to a delta-doped sheet would be remarkably broader than the measured one. We therefore assume that this peak is due to additional capacitance contributions of spatially localized states.<sup>24-26</sup> When the Fermi level crosses an interfacial level at sufficiently high reverse

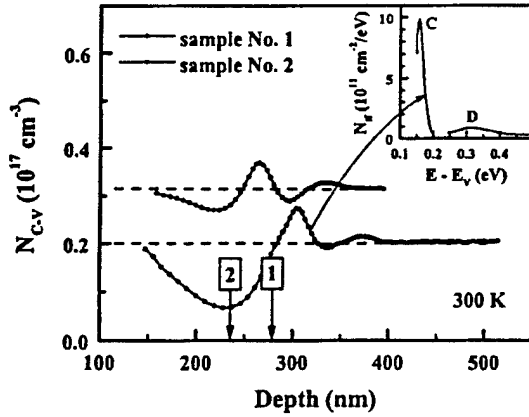


FIG. 4. Comparison of  $N_{C-V}$  vs depth profiles measured at 300 K on as-grown samples Nos. 1 and 2 with Ga(As, N) layer thicknesses of 50 and 10 nm, respectively. Their inverted interfaces are located at the same position, whereas the normal interfaces are displaced from 280 to 240 nm (marked by arrows). Doping levels are sketched by dashed lines. The profile of sample No. 1 is offset for clarity by  $-1 \times 10^{16} \text{ cm}^{-3}$ . In the inset, the energy distribution of the state density  $N_{if}$  at the normal interface is plotted for sample No. 1. The interfacial hole traps C and D are indicated.

biases, captured holes are released and give rise to the sharp carrier enhancement. That part of the depth profile, which is not described by the Poisson–Schrödinger solver used here, can therefore be employed for a spectroscopy of interface traps (release spectroscopy).<sup>25,26</sup> Applying the model of Ikeda *et al.*,<sup>25</sup> the energy distribution of the interface state density  $N_{if}(E)$  is calculated from

$$N_{if} = \left( \frac{N_{C-V}}{p} - 1 \right) \frac{\epsilon \epsilon_0 W(V)}{q^2 W_i [W(V) - W_i]}, \quad (3a)$$

and

$$E - E_V = E_F + \frac{q^2 p}{2 \epsilon \epsilon_0} [W(V) - W_i]^2, \quad (3b)$$

where  $W_i$  denotes the location of the interface and  $E_F$  the position of the Fermi level.

The release spectrum derived from Eqs. (3) for the inverted interface of the annealed structure is displayed in the inset of Fig. 3. Levels A and B, which are concentrated at the GaAs-on-Ga(As, N) interface with densities in the  $10^{10} \text{ cm}^{-2}$  range, appear at about 35 and 90 meV, respectively. Their origin is not clear yet. From our experiments it is also not apparent, whether both traps were formed during growth or during post-growth annealing. At room temperature, release spectra of these levels cannot be observed [Fig. 1(b)], because both levels are ionized at 0 V. Fitting the carrier density profile of the annealed sample No. 1 [Fig. 1(b)] measured at 300 K results in the same valence band offset as obtained from the fit of the 80 K data in Fig. 3.

The nodes found at 310 and 370 nm in Fig. 1(b) for the as-grown sample No. 1, are not related to real variations of the bulk hole density, but are also due to capacitance contributions of interfacial deep states.<sup>24–26</sup> Changing the thickness of the embedded Ga(As, N) layer from 50 (sample No. 1) to 10 nm (sample No. 2), the distance between both peaks remains constant (Fig. 4). According to Eq. (3b), the distance

between the interface position  $W_i$  and the node at a certain  $W$  depends mainly on the level energy  $(E - E_V)$ . Therefore, the two traps are linked with the same interface. The inverted interfaces of the two samples (Nos. 1 and 2), which are compared in Fig. 4, are located at the same position of 230 nm, but the normal interfaces are displaced (marked by the arrows). Both peaks of the  $N_{C-V}$  versus depth profiles shift in direct relation to the positions of the normal interface. Therefore, that part of the depth profiles can be evaluated by Eqs. (3) using  $W_i$  for the normal interface position.

The corresponding release spectrum for the as-grown sample No. 1 is depicted in the inset of Fig. 4. At the normal interface of as-grown GaAs/Ga(As, N)/GaAs structures we observe two trap levels C and D with energies of 0.16 and 0.32 eV, respectively. Their densities are in the  $10^{10} \text{ cm}^{-2}$  range. It is noteworthy that the same interfacial levels are also found by deep-level transient Fourier spectroscopy.<sup>29</sup> For donor-like interfacial traps, the apparent carrier enhancement in the  $C-V$  depth profile should be accompanied by an apparent depletion at lower reverse bias, contrary to acceptor-like traps.<sup>26</sup> Since such a reduction can be identified in Fig. 4 for level D, we further conclude that the signal at 0.32 eV is due to a donor-like interfacial level, i.e., the related trap is positively charged if occupied by a hole, but neutral in the empty state. From Fig. 1(b) it follows further that the interfacial level C can be suppressed by annealing, in contrast to the level D. The additional capacitance contributions originating from the deep states C and D at the normal interface are missing in depth profiles measured at 80 K [Fig. 1(a)], because the Fermi level at low temperatures does not cross these traps within the applied bias range.

The hole traps at the Ga(As, N)-on-GaAs interface are probably associated with the specific growth condition for GaAs close to the normal interface. The level D found at normal interfaces of as-grown samples clearly resembles the intrinsic hole trap H1, which is typically created in GaAs during irradiation by particles.<sup>30</sup> Level D may therefore be related to the operation of the rf nitrogen plasma source. The origin of trap C at the Ga(As, N)-on-GaAs interface is not yet clear. For potential applications, it is important to note that the concentration of the interfacial level C can be reduced by post-growth annealing.

### C. Variation of Ga(As, N) layer thickness

For Ga(As, N) layer thicknesses closer to the critical thickness, the amount of fixed charges at the inverted interface is remarkably enhanced in as-grown structures. Figure 5 reveals the carrier distributions measured at 80 and 300 K for sample No. 3 with 70 nm Be-doped Ga(As, N). For the as-grown heterostructure No. 3, the carrier deficit is found at 300 K to be about  $4.3 \times 10^{11} \text{ cm}^{-2}$ . It can be completely removed by annealing [Fig. 5(b)]. For the annealed sample, the depth profiles of the carrier concentration measured at 80 or 300 K can be best fitted neglecting any fixed charges at the interfaces. At sufficiently low temperatures, the valley on the GaAs side of the normal interface is clearly seen [Fig. 5(a)], but only after annealing, in contrast to the sample No. 1 with 50 nm Ga(As, N) studied in Fig. 1(a). The dashed lines in

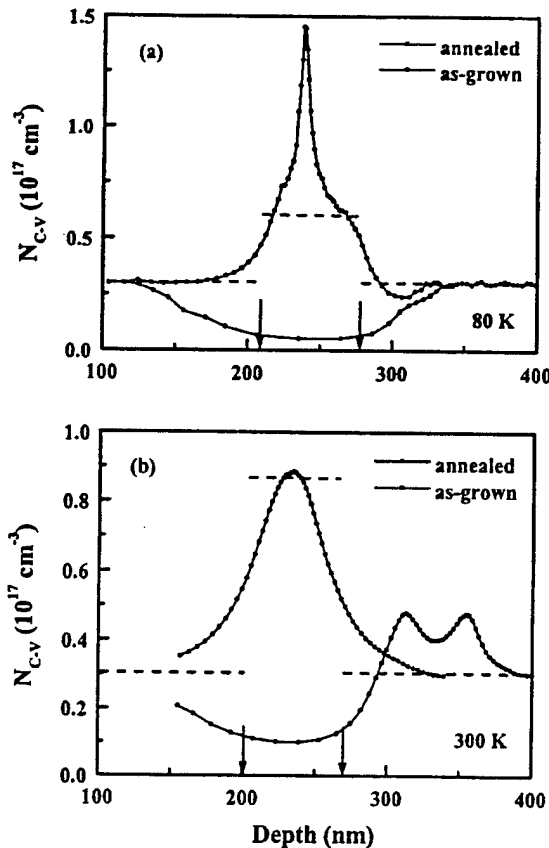


FIG. 5. Depth profiles of the apparent hole concentration  $N_{C-V}$  for sample No. 3 with 70 nm Be-doped Ga(As, N) measured (a) at 80 K and 10 kHz and (b) at 300 K and 1 MHz with test voltages  $V_{ac} = kT/q$ . Dashed lines indicate the doping levels of the individual layers as determined by the fitting procedure. The interface positions are marked by arrows.

Fig. 5 indicate the doping levels of the layers as obtained from the fitting procedure. In comparison with the not intentionally doped Ga(As, N) layer investigated in Fig. 1, it is obvious that additional holes are generated in Ga(As, N) by Be doping. Since the valence band offset for sample No. 3 is found to be only 9 meV, the depletion region on the GaAs side of the inverted interface is missing in Fig. 5(a) in agreement with the calculations.

From our experiments it is evident that the amount of fixed charges at the inverted interface of as-grown heterostructures increases with the thickness of the Ga(As, N) layer. In Fig. 6, the carrier deficit as measured by the  $C-V$  method at 300 K is plotted versus the layer thickness. The deficit changes by more than one order of magnitude for Ga(As, N) layer thicknesses between 10 and 70 nm. For larger thicknesses, the deficit rises superlinearly. Thus, the defects causing the carrier deficit at the inverted interface are strongly associated with the growth of strained Ga(As, N) and therefore most likely of intrinsic origin. It is a common phenomenon at  $X$ -on- $Y$  heterointerfaces that the formation of spatially localized electronic states is directly related to the growth process of the  $Y$  layer.<sup>31,32</sup> Defects, which are continuously generated during growth on the  $Y$  surface, may not be incorporated into the bulk of the epitaxial layer, but they are often deposited at the interface position, where material  $X$

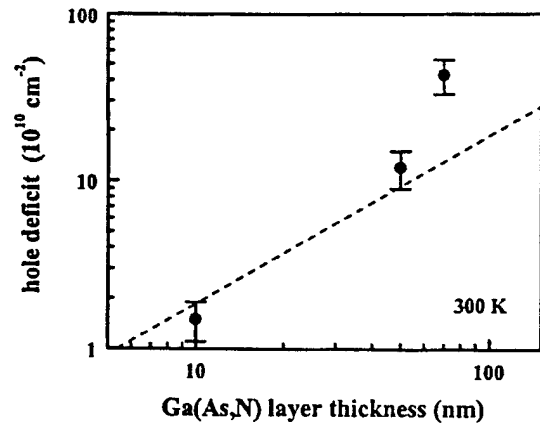


FIG. 6. Effective hole deficit of as-grown GaAs/Ga(As, N)/GaAs structures vs Ga(As, N) layer thickness. The deficit was measured by the  $C-V$  method at 300 K and 1 MHz. A linear relationship is sketched as a guide to the eye.

starts to grow.<sup>31,32</sup> Since the deficit in the studied heterostructures can be completely removed by annealing, we think that the spatially localized hole traps are annihilated by reactions between intrinsic defects, which are concentrated at the inverted interface. It is obvious that all partners, which are desired for the complete recombination of the interfacial defects, are available on the Ga(As, N) side.

#### IV. CONCLUSIONS

The electrical depth profile of isotype GaAs/Ga(As, N)/GaAs heterostructures shows that as-grown, strained Ga(As, N) layers are  $p$  type with hole concentrations of about  $3 \times 10^{16} \text{ cm}^{-3}$ . This density is stable during post-growth annealing. The valence band offset  $\Delta E_V$  between GaAs and GaAs<sub>0.97</sub>N<sub>0.03</sub> is found to be  $(11 \pm 2) \text{ meV}$ , i.e., the valence band edge in Ga(As, N) is higher than in GaAs, in agreement with recent theoretical results.<sup>22</sup> Together with the well-known band gap reduction of Ga(As, N), we can therefore conclude that the heterointerfaces are of type I, in contrast to the results obtained by x-ray photoelectron spectroscopy.<sup>20</sup> The latter method, which suffers from a large scatter of the data, delivers a value of  $-(19 \pm 53) \text{ meV}/\% \text{ N}$ .<sup>20</sup> The  $C-V$  method is apparently more suitable to evaluate heterointerfaces with very small band offsets. The electronic character of  $p$ -type GaAs/Ga(As, N) interfaces can be unambiguously identified at sufficiently low temperatures. We have no indication that the band offsets of the two interfaces are different.

Due to the lattice mismatch of around  $6 \times 10^{-3}$ , more and more defects are produced with increasing thickness at the growing Ga(As, N) surface, which are incorporated on the Ga(As, N) side of the inverted interface, i.e., when GaAs is grown on top. Their detailed intrinsic nature is still unknown. The dominant carrier depletion in the as-grown structures is due to these interfacial defects. It is technologically important that these distinct defects at the GaAs-on-Ga(As, N) interface can be fully removed by rapid thermal annealing after MBE growth. As far as the Ga(As, N)-on-GaAs interface is concerned, interfacial traps with densities

in the  $10^{10} \text{ cm}^{-2}$  range are observed, which are probably associated with the specific growth condition for GaAs close to the normal interface.

## ACKNOWLEDGMENTS

The authors are very grateful for the technical assistance of E. Wiebicke and are indebted to H. T. Grahn for comments and careful reading of the manuscript. This research was partially funded by DARPA and ARO through Contract No. DAAG 55-98-1-0437.

- <sup>1</sup>M. Kondow, K. Uomi, A. Niwa, T. Kitatani, S. Watahiki, and Y. Yazawa, *Jpn. J. Appl. Phys.*, Part 1 **35**, 1273 (1996).
- <sup>2</sup>S. Sato, Y. Osawa, and T. Saitoh, *Jpn. J. Appl. Phys.*, Part 1 **36**, 2671 (1997).
- <sup>3</sup>H. P. Xin and C. W. Tu, *Appl. Phys. Lett.* **72**, 2442 (1998).
- <sup>4</sup>T. Miyamoto, K. Takeuchi, T. Kageyama, F. Koyama, and K. Iga, *Jpn. J. Appl. Phys.*, Part 1 **37**, 90 (1998).
- <sup>5</sup>M. C. Larson, M. Kondow, T. Kitatani, K. Nakahara, K. Tamura, H. Inoue, and K. Uomi, *IEEE Photonics Technol. Lett.* **10**, 188 (1998).
- <sup>6</sup>A. Wagner, C. Ellmers, F. Höhnsdorf, J. Koch, C. Agert, S. Leu, M. Hofmann, W. Stolz, and W. W. Rühle, *Appl. Phys. Lett.* **76**, 271 (2000).
- <sup>7</sup>C. W. Coldren, M. C. Larson, S. G. Spruytte, and J. S. Harris, *Electron. Lett.* **36**, 951 (2000).
- <sup>8</sup>S. R. Kurtz, A. A. Allerman, E. D. Jones, J. M. Gee, J. J. Banas, and B. E. Hammons, *Appl. Phys. Lett.* **74**, 729 (1999).
- <sup>9</sup>M. Weyers, M. Sato, and H. Ando, *Jpn. J. Appl. Phys.*, Part 2 **31**, L853 (1992).
- <sup>10</sup>M. Weyers and M. Sato, *Appl. Phys. Lett.* **62**, 1396 (1993).
- <sup>11</sup>S.-H. Wei and A. Zunger, *Phys. Rev. Lett.* **76**, 664 (1996).
- <sup>12</sup>W. G. Bi and C. W. Tu, *Appl. Phys. Lett.* **70**, 1608 (1997).
- <sup>13</sup>T. Makimoto, H. Saito, T. Nishida, and N. Kobayashi, *Appl. Phys. Lett.* **70**, 2984 (1997).
- <sup>14</sup>K. Uesugi and I. Suemune, *Jpn. J. Appl. Phys.*, Part 2 **36**, L1572 (1997).
- <sup>15</sup>S. Francoeur, G. Sivaraman, Y. Qiu, S. Nikishin, and H. Temkin, *Appl. Phys. Lett.* **72**, 1857 (1998).
- <sup>16</sup>L. Malikova, F. H. Pollak, and R. Bhat, *J. Electron. Mater.* **27**, 484 (1998).
- <sup>17</sup>T. Prokofyeva, T. Sauncy, M. Seon, M. Holtz, Y. Qiu, S. Nikishin, and H. Temkin, *Appl. Phys. Lett.* **73**, 1409 (1998).
- <sup>18</sup>G. Pozina, I. Ivanov, B. Monemar, J. V. Thordson, and T. G. Andersson, *J. Appl. Phys.* **84**, 3830 (1998).
- <sup>19</sup>J. D. Perkins, A. Mascarenhas, Y. Zhang, J. F. Geisz, D. J. Friedman, J. M. Olson, and S. R. Kurtz, *Phys. Rev. Lett.* **82**, 3312 (1999).
- <sup>20</sup>T. Kitatani, M. Kondow, T. Kikawa, Y. Yazawa, M. Okai, and K. Uomi, *Jpn. J. Appl. Phys.*, Part 1 **38**, 5003 (1999).
- <sup>21</sup>S. Sakai, Y. Ueta, and Y. Terauchi, *Jpn. J. Appl. Phys.*, Part 1 **32**, 4413 (1993).
- <sup>22</sup>L. Bellaiche, S.-H. Wei, and A. Zunger, *Phys. Rev. B* **54**, 17568 (1996).
- <sup>23</sup>H. Kroemer, W.-Y. Chien, J. S. Harris, and D. D. Edwall, *Appl. Phys. Lett.* **36**, 295 (1980).
- <sup>24</sup>P. Blood and J. W. Orton, *The Electrical Characterization of Semiconductors: Majority Carriers and Electron States* (Academic, London, 1992).
- <sup>25</sup>E. Ikeda, H. Hasegawa, S. Ohtsuka, and H. Ohno, *Jpn. J. Appl. Phys.*, Part 1 **27**, 180 (1988).
- <sup>26</sup>J. Piprek, P. Krispin, H. Kostial, C. H. Lange, and K. W. Böer, *Phys. Status Solidi B* **173**, 661 (1992).
- <sup>27</sup>S. G. Spruytte, C. W. Coldren, A. F. Marshall, M. C. Larson, and J. S. Harris, *Mater. Res. Soc. Symp. Proc.* **595** (2000).
- <sup>28</sup>I.-H. Tan, G. L. Snider, L. D. Chang, and E. L. Hu, *J. Appl. Phys.* **68**, 4071 (1990).
- <sup>29</sup>P. Krispin, S. G. Spruytte, J. S. Harris, and K. H. Ploog (unpublished).
- <sup>30</sup>D. Pons and J. C. Bourgoin, *J. Phys. C* **18**, 3839 (1985).
- <sup>31</sup>P. Krispin, R. Hey, H. Kostial, and K. H. Ploog, *J. Appl. Phys.* **83**, 1496 (1998).
- <sup>32</sup>P. Krispin, M. Asghar, H.-P. Schönherr, H. Kostial, R. Nötzel, and K. H. Ploog, *Inst. Phys. Conf. Ser.* **166**, 155 (1999).

# Low-Threshold Oxide-Confining GaInNAs Long Wavelength Vertical Cavity Lasers

M. C. Larson, C. W. Coldren, *Member, IEEE*, S. G. Spruytte, H. E. Petersen, and J. S. Harris, *Fellow, IEEE*

**Abstract**—We report, for the first time, room temperature continuous-wave (CW) operation of GaInNAs vertical-cavity surface-emitting laser diodes emitting at a wavelength of  $1.2\ \mu\text{m}$  and grown all-epitaxially in a single step on a GaAs substrate. Oxide-apertured devices demonstrated CW threshold currents as low as 1 mA, slope efficiency above 0.045 W/A, and thermal impedance of 1.24 K/mW. Larger sized devices exhibited pulsed threshold current density of  $2\text{--}2.5\ \text{kA}/\text{cm}^2$  and slope efficiency above 0.09 W/A.

**Index Terms**—Long wavelength lasers on GaAs, semiconductor lasers, VCSELs, vertical-cavity surface-emitting lasers.

## I. INTRODUCTION

THE VERTICAL-CAVITY surface-emitting laser (VCSEL) is becoming an increasingly important optical source technology for short-haul optical fiber transmission systems because of its low-cost wafer-scale manufacturability and ease of packaging and coupling to optical fiber. Given the commercial success of GaAs-based 850-nm VCSELs, dramatic enhancements in bandwidth and distance can be achieved in conventional single- and multimode fiber by extending the emission wavelength to the 1300–1550 nm range. GaInNAs is a promising active layer material grown on GaAs that can achieve 1300-nm emission [1], [2], and both optically pumped [3]–[5] and electrically pulsed broad-area VCSELs [6], [7] have been realized. Here, we take advantage of the properties of GaAs-based materials (epitaxially grown thermally conductive high-contrast mirrors and AlAs-oxide current apertures [8]) to demonstrate low-threshold ( $\sim 1\ \text{mA}$ ) GaInNAs VCSELs emitting at a wavelength of 1200 nm under continuous-wave (CW) room-temperature operation.

## II. DEVICE STRUCTURE

The GaInNAs VCSEL device structure is shown schematically in Fig. 1, and consists of a GaInNAs multiple-quantum-well (MQW) active region embedded within a cavity spacer layer lying between a top and bottom mirror. The bottom mirror is a 22.5-period n-doped GaAs–AlAs

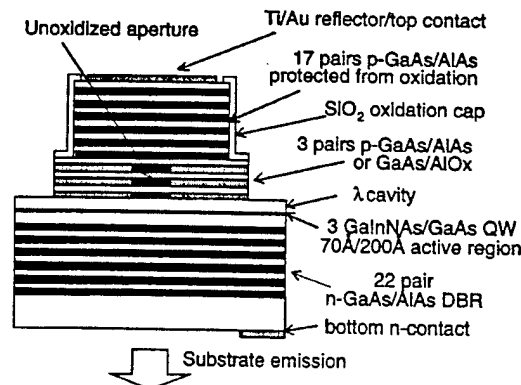


Fig. 1. Schematic diagram of GaInNAs vertical-cavity surface-emitting laser.

distributed Bragg reflector (DBR) designed for a center wavelength  $\lambda$  near 1200 nm. Centered within the GaAs  $\lambda$  cavity, which forms a p-i-n diode, is an active region of three 70-Å  $\text{Ga}_{0.3}\text{In}_{0.7}\text{N}_{0.02}\text{As}_{0.98}$  quantum wells separated by 200-Å GaAs barriers. This MQW active region exhibited threshold current density as low as  $600\ \text{A}/\text{cm}^2$  in 800- $\mu\text{m}$  long in-plane lasers [7]. The top mirror is a 20-period p-doped GaAs–AlAs DBR, on top of which is grown an additional p+ contact layer whose 630-Å thickness is chosen to appropriately allow reflection from the overlying 40-Å Ti/1200-Å Au contact electrode to add in phase with the DBR. The AlAs layers of the lowest three mirror periods of the top mirror also double as an oxide aperture upon selective lateral oxidation.

The epilayers were grown on an n+ GaAs substrate by molecular beam epitaxy using solid-source arsenic and a RF nitrogen plasma source. Si and Be were used as the n- and p-type dopants, respectively. Since binary materials were used for the mirror layers, a double-mesa fabrication process was required to control where the oxide aperture was located. The first mesa was formed by etching 17 mirror periods of the top mirror by chemically assisted ion beam etching. Three underlying periods were left unetched to allow for ease of fabrication using a simple timed etch, even if nonuniformity or overetching were present. This was followed by deposition of a  $\text{SiO}_2$  cap, which protected these etched layers from subsequent oxidation. Next, the remaining three mirror periods comprising the second mesa were etched to expose the AlAs for wet lateral oxidation, which formed square unoxidized apertures in the range of  $3.6\text{--}30\ \mu\text{m}$  on a side as measured by a microscope under near-IR illumination. After the top p-contact Ti–Au metallization, the n-type substrate was contacted by indium solder, and devices were mounted without heat sinking on a glass slide for optical emission through the substrate. Light output

Manuscript received July 14, 2000; revised August 16, 2000. This work was supported by the Department of Energy by University of California Lawrence Livermore National Laboratory under Contract W-7405-Eng-48 and by DARPA/ARO under Contract DAAG55-98-1-0437.

M. C. Larson and H. E. Petersen are with Lawrence Livermore National Laboratory, L-222, Livermore, CA 94551 USA.

C. W. Coldren is with Lawrence Livermore National Laboratory, Livermore, CA 94551 USA and also with Solid State and Photonics Lab, Stanford University, Stanford, CA 94305 USA.

S. G. Spruytte and J. S. Harris are with Solid State and Photonics Lab, Stanford University, Stanford, CA 94305 USA.

Publisher Item Identifier S 1041-1135(00)10473-2.

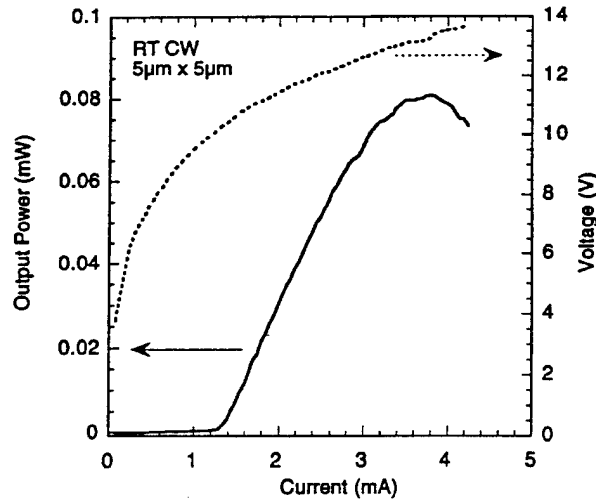


Fig. 2. Light output power and voltage versus injection current under room temperature CW operation.

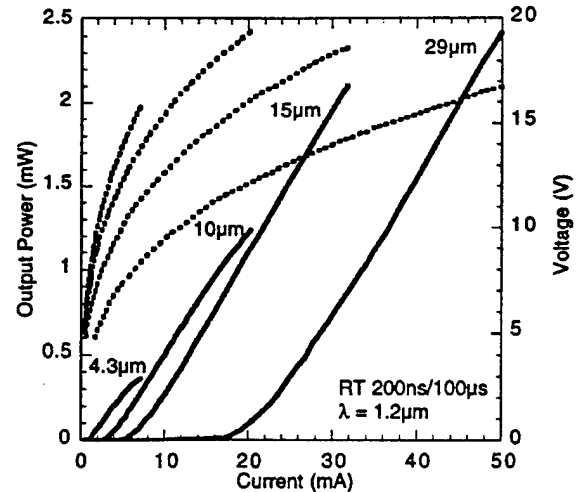


Fig. 4. Light output power and voltage versus injection current under pulsed operation for GaInNAs VCSELs with various aperture sizes.

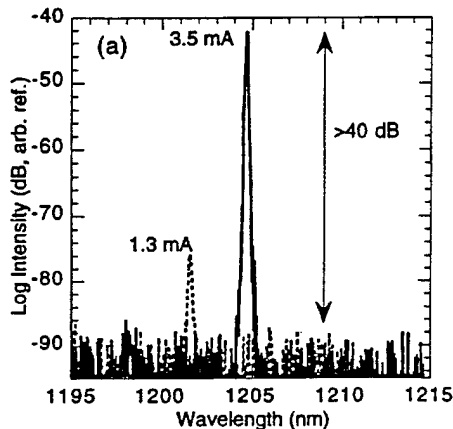


Fig. 3. (a) Emission spectra at 1.3 mA ( $\sim I_{th}$ ) and 3.5 mA ( $\sim 2.6 I_{th}$ ). (b) Wavelength shift and corresponding temperature rise versus average dissipated power. The data point near the origin is obtained by pulsed measurement; the others are CW.

was measured using a calibrated broad-area Ge photodiode or coupled into a graded-index lensed multimode fiber connected to an optical spectrum analyzer.

### III. RESULTS AND DISCUSSION

The output power and voltage vs. injection current for a device with a  $5 \mu\text{m} \times 5 \mu\text{m}$  aperture operating CW at room temperature is shown in Fig. 2. The threshold current is approximately 1.3 mA, and the slope efficiency is 0.045 W/A. An extremely high threshold voltage of 10.3 V resulted from unoptimized doping and composition-grading profiles at the heterointerfaces of the p-DBR. This created a large degree of self-heating, which limited the maximum output power to 0.080 mW at 3.8 mA. Fig. 3(a) shows the emission spectra at threshold, with a lasing wavelength of 1201.54 nm, and at 2.6 times threshold, with emission shifting to 1204.66 nm. The spectra indicate the device lased in a single transverse and longitudinal mode, and far above threshold, the sidemode

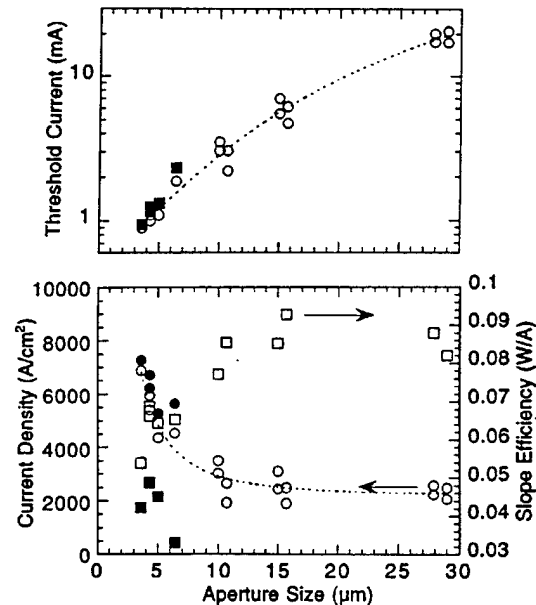


Fig. 5. Threshold current, threshold current density, and slope efficiency as a function of device size. Solid marks correspond to CW operation, unfilled ones are pulsed.

suppression ratio was in excess of 40 dB. As seen in Fig. 3(b), the wavelength shifted with dissipated power at a rate of 0.0924 nm/mW. Given a wavelength shift with temperature of 0.0743 nm/K obtained from broad-area pulsed VCSELs [9], this indicates a calculated temperature rise of approximately 60K above ambient temperature at peak output power and a thermal impedance of 1.24 K/mW. The fact that CW operation was possible in spite of the large excess power dissipation is indicative of the low temperature sensitivity of the GaInNAs MQW active region, coupled with the relatively high thermal conductivity of GaAs-based binary materials. CW laser operation also occurred for device sizes ranging from 3.6 to 6.4  $\mu\text{m}$ , with threshold currents from 0.94 to 2.3 mA and slope efficiency as high as 0.049 W/A.

Devices were also tested under pulsed operation to probe device characteristics as a function of aperture size independent of thermal effects. Fig. 4 shows the typical output power and voltage as a function of pulsed injection current (200 ns at 10 kHz) for several device sizes. Threshold current, current density, and slope efficiency versus aperture size are summarized for a wider range of devices in Fig. 5. Pulsed threshold current varied from 0.89 mA for 3.6- $\mu\text{m}$  devices to approximately 21 mA for 29- $\mu\text{m}$  sizes. Threshold current density was within the range of 2–2.5 kA/cm<sup>2</sup> at larger sizes, and slope efficiency above 0.09 W/A was achieved. Slope efficiency dropped for aperture sizes below 7  $\mu\text{m}$ , which was likely due to optical scattering, and current density rose to nearly 7 kA/cm<sup>2</sup> for the smallest (3.6  $\mu\text{m}$ ) devices. Optimization of the oxide aperture thickness, shape, and placement with respect to the optical standing wave should also reduce this excess scattering for small devices in a similar fashion as it has for near-IR VCSELs [10].

Characteristics of VCSELs operating CW are also included in Fig. 5. Under CW operation, efficiency fell by approximately 30% compared to pulsed mode due to self heating, accompanied by a slight increase in threshold current. This behavior is consistent with previous reports on pulsed etched-pillar devices at high temperature [6], [9], where the temperature sensitivity of the slope efficiency was more pronounced than that of the threshold current. One possible explanation is temperature-dependent absorption in the DBRs combined with gain/cavity-mode detuning effects.

#### IV. CONCLUSION

We have demonstrated low-threshold GaInNAs VCSELs with an emission wavelength of 1200 nm operating CW at room temperature. Devices exhibited milliamp threshold currents and peak output powers above 0.08 mW. Future improvements in performance should be readily achieved by further adapting well-established 850-nm VCSEL technology. Namely, higher output power will be possible by reducing the

resistance of the p-DBR through finer control of composition grading and doping, and lower threshold current by reducing scattering in small-aperture devices. This will also improve high-temperature performance through reduced self-heating. Finally, 1300-nm emission should be achieved by increasing the indium and/or nitrogen content of the GaInNAs-GaAs MQW active layer.

#### REFERENCES

- [1] M. Kondow, T. Kitatani, S. Nakatsuka, M. C. Larson, K. Nakahara, Y. Yazawa, M. Okai, and K. Uomi, "GaInNAs: A novel material for long wavelength semiconductor lasers," *IEEE J. Select. Topics Quantum Electron.*, vol. 3, pp. 719–730, June 1997.
- [2] S. Sato, Y. Osawa, T. Saitoh, and I. Fujimura, "Room-temperature pulsed operation of 1.3  $\mu\text{m}$  GaInNAs/GaAs laser diode," *Electron. Lett.*, vol. 33, no. 16, pp. 1386–1387, July 1997.
- [3] M. C. Larson, M. Kondow, T. Kitatani, Y. Yazawa, and M. Okai, "Room temperature continuous-wave photopumped operation of 1.22- $\mu\text{m}$  GaInNAs/GaAs single quantum well vertical-cavity surface-emitting laser," *Electron. Lett.*, vol. 33, pp. 959–960, 1997.
- [4] M. C. Larson, M. Kondow, T. Kitatani, K. Tamura, and M. Okai, "Photopumped lasing at 1.25  $\mu\text{m}$  of GaInNAs-GaAs multiple-quantum-well vertical-cavity surface-emitting lasers," *IEEE Photon. Technol. Lett.*, vol. 9, pp. 1549–1551, Dec. 1997.
- [5] C. Ellmers, F. Hohnsdorf, J. Koch, C. Agert, S. Leu, D. Karauskaj, M. Hofman, W. Stolz, and W. W. Ruhle, "Ultrafast GaInNAs/GaAs vertical-cavity surface-emitting laser for the 1.3  $\mu\text{m}$  wavelength regime," *Appl. Phys. Lett.*, vol. 74, no. 16, Apr. 19, 1999.
- [6] M. C. Larson, M. Kondow, T. Kitatani, K. Nakahara, K. Tamura, H. Inoue, and K. Uomi, "GaInNAs/GaAs long-wavelength vertical-cavity surface-emitting laser diodes," *IEEE Photon. Technol. Lett.*, vol. 10, pp. 188–190, Feb. 1998.
- [7] C. W. Coldren, M. C. Larson, S. G. Spruytte, and J. S. Harris Jr., "1200 nm GaAs based vertical cavity lasers employing GaInNAs multiple quantum well active regions," *Electron. Lett.*, vol. 36, no. 11, pp. 951–952, May 25, 2000.
- [8] D. L. Huffaker, D. G. Deppe, K. Kumar, and T. J. Rogers, "Native-oxide defined ring contact for low threshold vertical-cavity lasers," *Appl. Phys. Lett.*, vol. 65, no. 1, pp. 97–99, July 4, 1994.
- [9] C. W. Coldren, M. C. Larson, S. G. Spruytte, H. E. Garrett, and J. S. Harris, "Pulsed 25–108°C operation of GaInNAs multiple quantum well vertical cavity lasers," in *Proc. Lasers and Electro-optics Conf. (CLEO '00)*, San Francisco, CA, 2000, Paper ThL1.
- [10] E. R. Hegblom, N. M. Margalit, A. Fiore, and L. A. Coldren, "Small efficient vertical cavity lasers with tapered oxide apertures," *Electron. Lett.*, vol. 34, pp. 895–897, Apr. 30, 1998.